NACA TN 2750

NATIONAL ADVISORY COMMITTEE FOR AERONAUTICS

TECHNICAL NOTE 2750

MATRIX AND RELAXATION SOLUTIONS THAT DETERMINE SUBSONIC THROUGH FLOW IN AN AXIAL-FLOW GAS TURBINE

By Chung-Hua Wu

Lewis Flight Propulsion Laboratory
Cleveland, Ohio

PROPERTY FAIRCHILD
ENGINEERING LIBRARY

Washington
July 1952

1S

2402

NATIONAL ADVISORY COMMITTEE FOR AERONAUTICS

TECHNICAL NOTE 2750

MATRIX AND RELAXATION SOLUTIONS THAT DETERMINE SUBSONIC THROUGH FLOW IN AN AXIAL-FLOW GAS TURBINE

By Chung-Hua Wu

SUMMARY

A method recently developed for determining the steady flow of a nonviscous compressible fluid along a relative stream surface between adjacent blades in a turbomachine was applied to investigate the subsonic through flow in a single-stage axial-flow gas turbine. A free-vortex type of variation in tangential velocity was prescribed along the stream surface. Cylindrical bounding walls were specified in order to avoid radial flow at the walls. The flow variations on the stream surface for incompressible and compressible flows were obtained by using the relaxation method with hand computation and the matrix method on both an IBM Card Programmed Electronic Calculator and a UNIVAC.

In all solutions considered in this investigation, convergence was obtained without difficulty. A comparison between the relaxation and the matrix methods showed that more accurate results were obtained with the matrix method in a shorter interval of time. The results of these accurate calculations provide a basis for evaluation of simpler, more approximate methods for computing subsonic through flow in turbines.

Considerable radial flow was obtained for both incompressible and compressible flows because of the radial twist of the stream surface required by the prescribed velocity diagram and the compressibility of the gas; the radial twist of the stream surface and the compressibility of the gas had equally important effects, and the nonlinear nature of the equations defining the flow was quite evident. The shape of the stream surface was found to be sensitive to the axial position of the radial element of the stream surface in the stator. When the radial element of the stream surface in the rotor was near the midaxial position in the rotor, a large negative gradient of axial velocity was observed in all cases ahead of the rotor.

INTRODUCTION

In the design of gas turbines having relatively long blades in the radial direction, a first approximation of the radial variation of the state of the gas is commonly obtained by assuming the gas to be nonviscous and to flow on cylindrical surfaces. Axial symmetry is assumed in such one-dimensional solutions for the radial variation in the gas state upstream and downstream of a blade row and they are usually referred to as the "simple-radial-equilibrium" or "simplified-radial-equilibrium" solutions (see references 1 and 2 for examples). Even turbines designed from a free-vortex velocity diagram, however, have considerable radial displacement of gas particles across the blade row due to the compressibility of the gas; this displacement, of course, violates the assumption of flow on cylindrical surfaces. The radial displacement of gas particles across the blade row and the curvature in the streamline caused by the radial motion have a significant effect on the radial variation in the gas state (see reference 2). 2402

Several through-flow methods have been developed to consider both radial and axial variations in flow conditions (see, for example, references 2 and 3). In these methods an infinite number of blades and a nonviscous fluid are assumed. The interpretation of such a solution, its modification for any finite number of thick blades, and its extension to a complete three-dimensional solution for nonviscous fluids are given in reference 4. In actual turbines, the motion of the gas is further complicated by the secondary flow caused by the boundary layers along the hub and casing walls (for example, reference 5). Nevertheless, it is believed that the detailed flow analysis based on an assumption of a nonviscous gas will permit a clearer understanding of the individual contributions to the complete flow and help to explain the development of the viscous boundary layer along the walls.

The theoretical method of reference 4 for obtaining a complete three-dimensional solution is based on an appropriate combination of a number of mathematically two-dimensional flows on two kinds of relative stream surface. The first kind of relative stream surface extends from the suction surface of one blade to the pressure surface of the adjacent blade and deviates, in general, from a surface of revolution about the axis of the turbomachine; in reference 4 this surface is called S_1. The second kind of relative stream surface extends from hub to casing and roughly approximates the shape of the mean camber surface of the blades; in reference 4 this surface is called S_2. The equations defining the flow on these two kinds of stream surface are, however, similar and the methods of successive approximation used in their solution are essentially the same. The mechanics of obtaining a numerical solution of either of these two-dimensional problems by the methods of reference 4 has not previously been investigated. If convergence of one of these

two-dimensional solutions can be obtained without difficulty, the other solution should then converge as well. The method of reference 4 will then very likely be practical for analyzing three-dimensional flows of compressible nonviscous fluids in turbomachines having finite numbers of thick blades and arbitrary hub and casing shapes.

The primary objective of this investigation made at the NACA Lewis laboratory is to study in detail the technique of solving for the subsonic flow along a relative stream surface of the second kind (S_2) by using the methods of references 4 and 6. At the same time, of course, the effects of compressibility and radial twist of the stream surface are obtained; the examination of these effects therefore constitutes the secondary purpose of this investigation. If highly accurate solutions can be obtained in this way, these solutions will provide a basis for evaluation of other simpler but more approximate solutions for subsonic through flow in turbines.

2402

For these calculations, a single-stage axial-flow turbine was selected as the machine type to be analyzed. The annulus walls were chosen to be cylindrical and to have a hub-tip radius ratio of 0.6. The radial distribution of the tangential component of velocity was of the free-vortex type. The turbine-work parameter $-\Delta H/U_t^2$ was 0.96 where $-\Delta H$ represents the stagnation-enthalpy drop and U_t, the blade-tip speed. The tangential component of velocity at the rotor exit was assigned equal to zero. For a compressible fluid, the assigned conditions resulted in an absolute Mach number of 0.99 at the root and exit of the stator and a relative Mach number of about 0.70 at the root and entrance of the rotor. The effects of radial blade force were varied by changing (1) the axial distribution of aerodynamic loading and (2) the axial location of the radial element of the stream surfaces in the stator.

The following three methods were employed in making the calculations:

(1) Relaxation method with the use of a hand-operated desk calculator

(2) Matrix method on an IBM Card Programmed Electronic Calculator

(3) Matrix method on a UNIVAC

The matrix factors obtained in the matrix solutions can be used for similar calculations for compressors and turbines which have a constant hub-tip radius ratio of 0.6.

SYMBOLS

The following symbols are used in this report. (Bold symbols indicate vectors on the stream surface; nonbold symbols indicate the components of these vectors.)

a	velocity of sound
B	variable defined by equation (2c)
${}^{m}_{4}B^{i}_{j}$	differentiation coefficients in equation (26) used to multiply function value at grid point j to give m^{th} derivative at grid point i using polynomial of fourth degree
$[C],[E],[F],$ $[G],[L],[u]$	square matrices
$\frac{D}{Dt}$	differentiation with respect to time following motion of gas particle
$\mathbf{F}$	vector having dimensions of force per unit mass of gas; defined by equation (6)
H	total, or stagnation, enthalpy per unit mass of gas, $h + \frac{V^2}{2}$; $H^* U_t^2$
h	enthalpy per unit mass of gas
i,j,k	grid points
M	Mach number
N	nonhomogeneous term of principal equation as given in equation (5)
$\mathbf{n}$	unit vector normal to stream surface
p	static pressure of gas
q	any dependent variable
R	gas constant
r	radial distance, $r^* r_t$

2402

s	entropy per unit mass of gas, s^*R
T	temperature of gas
t	time
U	velocity of blade at radius r
V	absolute gas velocity, V^*U_t
W	relative gas velocity, W^*U_t
z	axial distance, z^*r_t
$\{\alpha\},\{\beta\},\{\psi\}$	column matrices
γ	ratio of specific heats, 1.33
δ_r,δ_z	grid spacing in r- and z-directions, respectively; $\delta_r^*r_t$, $\delta_z^*r_t$
ρ	mass density, $\rho^*\rho_{T,i}$
Σ,Φ	general variables used in density table
φ	angular position
ψ	stream function, $\psi^*\rho_{T,i}U_tr_t^2$
ω	angular speed of blade

Subscripts:

e	exit
h	hub
i	inlet
j	grid point
o	refers to position where stream surface has a radial element or where $F_r = 0$
r	radial component
T	total, or stagnation, state

t tip

u tangential, or circumferential, component

z axial component

Superscripts:

i,j,k grid points

* dimensionless value

2402

EQUATIONS GOVERNING FLOW ON A RELATIVE STREAM SURFACE BETWEEN TWO ADJACENT BLADES

The present report is concerned with the inverse solution (design problem) for the steady compressible flow on a relative stream surface about midway between two adjacent blades (see fig. 1). The shape of this stream surface is not known in advance but the variation in tangential velocity of the gas and the position of the radial element of the surface are prescribed in the design. The shape of the stream surface as well as the state of the gas flowing along the surface is described by the two independent variables r and z.

In reference 4, the following continuity equation for steady flow on the stream surface is obtained:

$$\frac{\boldsymbol{\partial}(rB\rho W_r)}{\boldsymbol{\partial} r} + \frac{\boldsymbol{\partial}(rB\rho W_z)}{\boldsymbol{\partial} z} = 0 \tag{1}$$

In equation (1) the bold partial derivative sign denotes the rate of change of the dependent variable on the stream surface with respect to the independent variable and is related to the ordinary partial derivative with respect to the coordinates r, φ, and z as follows:

$$\frac{\boldsymbol{\partial} q}{\boldsymbol{\partial} r} = \frac{\partial q}{\partial r} - \frac{n_r}{n_u}\frac{1}{r}\frac{\partial q}{\partial \varphi} \tag{2a}$$

$$\frac{\boldsymbol{\partial} q}{\boldsymbol{\partial} z} = \frac{\partial q}{\partial z} - \frac{n_z}{n_u}\frac{1}{r}\frac{\partial q}{\partial \varphi} \tag{2b}$$

The angular variation of the variable is thus implicitly included although its value can be calculated only after the shape of the stream

surface is obtained in the solution. The variable B in equation (1) is related to the angular variation of the gas velocities and the shape of the stream surface by

$$\ln \frac{B}{B_i} = \int_{t_i}^{t} \left(\frac{n_r}{n_u r} \frac{\partial W_r}{\partial \varphi} + \frac{1}{r} \frac{\partial W_u}{\partial \varphi} + \frac{n_z}{n_u r} \frac{\partial W_z}{\partial \varphi} \right) dt \tag{2c}$$

2402

This variable B can also be interpreted as a variable angular thickness of a thin stream sheet whose mean surface is the stream surface shown on figure 1 (reference 4). Because B along the mean stream surface is very closely related to the ratio of circumferential channel width to pitch (reference 7), it can be approximately estimated in the design by considering desirable axial and radial variations in blade thickness required to provide, for example, adequate strength and a cooling passage of sufficient size; with these variations taken into account, B can then be used in the design calculation of the mean stream surface. For the limiting case of an infinite number of blades of zero thickness, B becomes a constant and is taken equal to 1.

Equation (1) is the necessary and sufficient condition that a stream function ψ exists with

$$\frac{\partial \psi}{\partial r} = rB\rho W_z \tag{3}$$

$$\frac{\partial \psi}{\partial z} = -rB\rho W_r \tag{4}$$

With the tangential velocity of the gas specified, the subsonic flow of the gas is obtained by the solution of ψ in the following principal equation, which is obtained from the equation of motion in the radial direction with the use of relations (3) and (4):

$$\frac{\partial^2 \psi}{\partial r^2} - \frac{1}{r} \frac{\partial \psi}{\partial r} + \frac{\partial^2 \psi}{\partial z^2} = N \tag{5}$$

where

$$N = \frac{1}{B\rho} \left[\frac{\partial (B\rho)}{\partial r} \frac{\partial \psi}{\partial r} + \frac{\partial (B\rho)}{\partial z} \frac{\partial \psi}{\partial z} \right] - \frac{(rB\rho)^2}{\partial \psi / \partial r} \left[\frac{V_u}{r} \frac{\partial (V_u r)}{\partial r} - \frac{\partial H}{\partial r} + T \frac{\partial s}{\partial r} + F_r \right]$$

In equation (5), F_r is the radial component of a vector F, which is defined as follows:

$$\mathsf{F} = -\frac{1}{n_u r}\left(\frac{\partial h}{\partial \varphi} - T\frac{\partial s}{\partial \varphi}\right)\mathsf{n} = -\frac{1}{n_u r \rho}\frac{\partial p}{\partial \varphi}\mathsf{n} \tag{6}$$

For the limiting case of an infinite number of blades, F becomes the blade force. For the evaluation of F_r, which represents the influence of the radial twist of the stream surface and of the circumferential pressure gradient on the gas flow, the other components of F are first computed by the equation of motion in the tangential and axial directions: 2402

$$F_u r = \frac{1}{rB\rho}\left[-\frac{\partial \psi}{\partial z}\frac{\partial(V_u r)}{\partial r} + \frac{\partial \psi}{\partial r}\frac{\partial(V_u r)}{\partial z}\right] \tag{7}$$

$$F_z = -\frac{W_u}{r}\frac{\partial(V_u r)}{\partial z} - T\frac{\partial s}{\partial z} + \frac{\partial\psi/\partial z}{\partial\psi/\partial r}\left[\frac{\partial H}{\partial r} - \omega\frac{\partial(V_u r)}{\partial r}\right] -$$

$$\frac{1}{(rB\rho)^2}\frac{\partial \psi}{\partial z}\left\{\frac{\partial^2\psi}{\partial r^2} - \frac{1}{r}\frac{\partial \psi}{\partial r} + \frac{\partial^2\psi}{\partial z^2} - \frac{1}{B\rho}\left[\frac{\partial(B\rho)}{\partial r}\frac{\partial \psi}{\partial r} + \frac{\partial(B\rho)}{\partial z}\frac{\partial \psi}{\partial z}\right]\right\} \tag{8}$$

The component F_r is then obtained by the use of the following equation, which is derived from the integrability condition, which insures that the stream surface to be obtained is a continuous integral surface:

$$F_r = F_u r \int_{z_o}^{z} \frac{\partial}{\partial r}\left(\frac{F_z}{F_u r}\right) dz \tag{9}$$

The radial derivative of entropy s in equation (5) is determined from its radial distribution at the inlet and the following condition of the constancy of s along a streamline on the stream surface for reversible adiabatic flow:

$$\frac{Ds}{Dt} = 0 \tag{10}$$

The radial derivative of H in equation (5) is determined from the inlet variation and the following equation:

$$\frac{DH}{Dt} = \omega \frac{D(V_u r)}{Dt} \tag{11}$$

2402 Equation (11) is obtained (reference 4) by the use of the equation of motion on the stream surface and the following equation expressing the orthogonal relation between the resultant relative velocity and the surface normal $\mathbf{n}$ or its parallel vector $\mathbf{F}$:

$$W_r F_r + W_u F_u + W_z F_z = 0 \tag{12}$$

Because the three equations of motion have already been employed in the solution, there is only one more independent relation in equations (11) and (12). In the following, equation (11) is used and is considered to represent the orthogonal relation (12).

The variation of density included in N in equation (5) is determined from the ψ-derivatives by use of the following relation between density, enthalpy, and entropy, between the local static condition and the total condition at the inlet:

$$\frac{\rho}{\rho_{T,i}} = \left[\frac{H}{H_i} - \frac{(V_u r)^2}{2H_i r^2} - \frac{\left(\frac{\partial\psi}{\partial r}\right)^2 + \left(\frac{\partial\psi}{\partial z}\right)^2}{2H_i (rB\rho)^2}\right]^{\frac{1}{\gamma-1}} e^{s^*_{T,i} - s^*} \tag{13}$$

PRESCRIBED DESIGN CONDITIONS

In the present study of the through flow in a gas turbine, the effects of some of the design variables are considered. Cylindrical bounding walls are specified in order to avoid radial flow at the walls. The meridional section of the turbine is shown in figure 2. A hub-tip radius ratio of 0.6 and a blade aspect ratio of 2.67 (which is based on axial chord and corresponds to the blade-row aspect ratio of 2 used in reference 2) are chosen in order to compare some of the results with those previously obtained in reference 2 by an approximate method.

Flow conditions were computed for six sets of assigned conditions. These sets of conditions are designated cases A, B, C, D, E, and F and are summarized in the following table:

Case	Fluid	Loading distribution	Axial location in stator of radial element of stream surface z_o^*
A	Incompressible	Uniform	0.0675
B	Incompressible	Nonuniform	.0625
C	Compressible	Nonuniform	(F_r neglected)
D	Compressible	Nonuniform	.0625
E	Compressible	Nonuniform	0
F	Compressible	Nonuniform	.1500

2402

The prescribed variation of tangential velocity, or the angular momentum per unit mass of gas $V_u^* r^*$, is such that at a constant-z plane, $V_u^* r^*$ on the stream surface is constant with respect to r^*; and at all fixed values of r^*, the variation of $V_u^* r^*$ on the stream surface with respect to z^* is as shown in figure 3. Two kinds of variation with respect to z^* are considered. The dashed line shows a linear variation, and the solid line shows a composite variation in which a constant rate is maintained for the first half of the blade chord and a rate linearly decreasing to zero is used for the second half. These two variations are called uniform and nonuniform loading, respectively. In both cases the total change of $V_u r$ divided by $U_t r_t$ (or $-\Delta H/U_t^2$) across the blade row is 0.96, which is used in reference 2. The expressions for the dimensionless specific angular momentum are as follows:

(a) Uniform loading

Stator: $0 \leq z^* \leq 0.15$,

$$\frac{\partial(V_u^* r^*)}{\partial z^*} = \frac{0.96}{0.15} \tag{14}$$

$$V_u^* r^* = \frac{0.96}{0.15} z^* \tag{15}$$

2402

Rotor: $0.20 \leq z^* \leq 0.35$,

$$\frac{\partial(V_u^* r^*)}{\partial z^*} = -\frac{0.96}{0.15} \tag{16}$$

$$V_u^* r^* = \frac{0.96}{0.15}(0.35 - z^*) \tag{17}$$

(b) Nonuniform loading

Stator: $0 \leq z^* \leq 0.075$,

$$\frac{\partial(V_u^* r^*)}{\partial z^*} = \frac{4}{3}\frac{0.96}{0.15} \tag{18}$$

$$V_u^* r^* = \frac{4}{3}\frac{0.96}{0.15} z^* \tag{19}$$

$0.075 \leq z^* \leq 0.15$,

$$\frac{\partial(V_u^* r^*)}{\partial z^*} = \frac{8}{3}\frac{0.96}{0.15}\left(1 - \frac{z^*}{0.15}\right) \tag{20}$$

$$V_u^* r^* = -0.32 + \frac{4}{3} \times 0.96\left[2\frac{z^*}{0.15} - \left(\frac{z^*}{0.15}\right)^2\right] \tag{21}$$

Rotor: $0.20 \leq z^* \leq 0.275$,

$$\frac{\partial(V_u^* r^*)}{\partial z^*} = -\frac{4}{3}\frac{0.96}{0.15} \tag{22}$$

$$V_u^* r^* = 0.96 - \frac{4}{3}\frac{0.96}{0.15}(z^* - 0.2) \tag{23}$$

$0.275 \leq z^* \leq 0.35$,

$$\frac{\partial(V_u^* r^*)}{\partial z^*} = -\frac{8}{3}\frac{0.96}{0.15}\left(1 - \frac{z^* - 0.2}{0.15}\right) \tag{24}$$

$$V_u^* r^* = 1.28 - \frac{4}{3} \times 0.96 \left[2 \frac{z^*}{0.15} - \left(\frac{z^* - 0.2}{0.15} \right)^2 \right] \quad (25)$$

For a given axial distribution of tangential velocity, a change in the axial location of the radial element of the stream surface will alter the radial and axial distributions of both axial and radial velocities and thereby change the shape of the stream surface. In the rotor, the axial location of the radial element of the relative stream surface is 45 percent of the axial blade chord from the leading edge ($z_o^* = 0.2675$) for case A and 41.7 percent ($z_o^* = 0.2625$) for cases B, D, E, and F. 2402

With this prescribed axial variation in $V_u r$, the radial derivative of $V_u r$ contained in the equations given in the preceding section drops out. Also, for the present investigation, the inlet flow is considered to be uniform in entropy and total enthalpy. Then, for adiabatic frictionless flow, the radial and axial derivatives of s vanish. The radial derivative of H also vanishes for the specified inlet condition and $V_u r$.

For the present investigation, B is taken to be a constant (a value of 1 is used in the calculation). In a sense, the solutions thus obtained do not depend on any particular blade configurations. But the solution is correct only for those bladings whose geometrical configuration is such that the angular thickness of the mean stream sheet is essentially constant. It also gives the limiting solution for an infinite number of infinitely thin blades. To interpret the results obtained as this limiting solution, the prescribed variation of $V_u r$ corresponds exactly to the free-vortex type with $\partial(V_u r)/\partial r$ equal to zero. For the general interpretation of the results obtained as the solution for the flow along a mean stream surface (subject to the assumed constant value of B), the prescribed condition that $\partial(V_u r)/\partial r$ be equal to zero does not give $\partial(V_u r)/\partial r$ equal to zero.

The inlet flow of the turbine example given in reference 2 is used in the present investigation and is as follows:

$$V_i^* = \frac{V_i}{U_t} = 0.650$$

$$M_i = 0.308$$

For this Mach number,

$$\rho_i^* = \frac{\rho_i}{\rho_{T,i}} = 0.95033$$

$$H_i^* = \frac{H_i}{U_t^{\,2}} = 12.546$$

2402

METHOD OF SOLUTION

The principal equation to be solved is equation (5). This partial differential equation is first replaced by a number of finite-difference equations representing the differential equation at a number of grid points covering the domain. Because of the nonlinear nature of the problem, these equations are solved by the general method of successive approximations. In each cycle of calculation, the nonhomogeneous term N is evaluated by employing any appropriate approximate solution at the start and by using equations (7) to (11) and equation (13) together with the flow variation obtained in the preceding cycle; the results are then taken as given values in the solution of ψ in the following cycle. The solution of ψ from the finite-difference form of the principal equation is obtained by the relaxation method (reference 8) in the modified form as given in reference 6 and by the matrix method discussed in reference 6. The accuracy of the solution depends on the accuracy of the finite-difference representation of the partial differential equation, the size of the residual left in the solution of ψ, and the number of cycles completed for convergence.

Choice of Grid System and Degree of Polynomial Representation

In these calculations, a single grid size was used for both the relaxation and the matrix calculations. The results of reference 2 were useful in selection of the grid size. From the results obtained in reference 2, the stream function ψ is expected to increase smoothly with respect to radius at constant-z planes and to vary approximately as a sine curve with respect to z at constant r-values. With the necessity of covering a large domain in order to satisfy the boundary conditions given far upstream of the stator and far downstream of the rotor, and with such a smooth variation of ψ over the domain, the use of a fourth-degree polynomial representation rather than of the usual second-degree one is suggested so that the number of grid points may be reduced. From experience gained while obtaining relaxation solutions, a final grid size of 0.05 r_t in the radial direction and

0.025 r_t in the axial direction in the meridional plane are used (fig. 4). These grid points on the meridional plane are for reference, or recording, purposes only. The variables involved in the solution are those on the stream surface (fig. 4).

The use of this grid size gives seven radial and axial stations on the stream surface between the hub and the casing and across each blade row. With the present variation of ψ in the radial direction, sufficiently accurate results are expected for radial derivatives. The accuracy of the axial derivatives is analyzed for a simple sinusoidal variation in the axial direction with a period of 20 δ_z, and the fourth-degree polynomial representation is found to give first- and second-order derivatives accurate to within 0.02 percent.

For simplicity (in order to give a uniform formula in the z-direction), the same grid size in the z-direction is used for the entire domain. It is found in the relaxation solution that the radial distribution of ψ had no axial variation in the first five significant figures after eight of these z-stations either upstream of the stator or downstream of the rotor. The matrix factors for matrix solutions therefore cover a range of z^* varying from -0.5 to 0.85, which includes 10 stations each way upstream of the stator and downstream of the rotor. The order of matrices is thus $7 \times 55 = 385$, which is also the total number of interior grid points.

At the first and the last z-stations and a few stations nearby, sufficiently accurate z-derivatives can be obtained by the use of a three-point differentiation formula. For simplicity in setting up the matrix factorization, however, the same central-point fourth-degree differentiation formulas are used for the entire domain. The use of these formulas means that the same boundary values of ψ are used for the two stations outside the first ($z^* = -0.5$) and the last ($z^* = 0.85$) z-stations.

Finite-Difference Form of Principal Equation

With the grid sizes of 0.05 and 0.025 chosen for δ_r^* and δ_z^*, respectively, the differentiation coefficients for the first- and the second-order derivatives are computed. If these coefficients at grid point i are denoted by ${}^{1}_{4}B^{i}_{j}$ and ${}^{2}_{4}B^{i}_{j}$, respectively, the finite-difference form of the principal equation at any grid point i becomes

$$\sum_{j=0}^{4}\left({}^{2}_{4}B^{i}_{j} - \frac{1}{r^{i}}\,{}^{1}_{4}B^{i}_{j}\right)\psi^{j} + \sum_{k=0}^{4}{}^{2}_{4}B^{i}_{k}\,\psi^{k} = N^{i} \tag{26}$$

where ψ^{j} and ψ^{k} denote the values of ψ on the stream surface corresponding to the grid points along constant-z and constant-r lines on the meridional plane, respectively (fig. 4).

2402

Calculation of Boundary Values of ψ

The value of ψ along the hub is chosen to be zero. The value of a dimensionless ψ along the casing is chosen as follows: At station i-i, with the use of equation (3),

$$\psi_t^* = \frac{\psi_t}{\rho_{T,i}\,U_t\,r_t^{\,2}} = \frac{\displaystyle\int_{r_h}^{r_t}\left(\frac{\partial\psi}{\partial r}\right)_i dr_i}{\rho_{T,i}\,U_t\,r_t^{\,2}}$$

$$= \frac{B_i\rho_i\,V_{z,i}\,\dfrac{r_t^{\,2}-r_h^{\,2}}{2}}{\rho_{T,i}\,U_t\,r_t^{\,2}} = \frac{1}{2}B_i\,\rho_i^*\,V_{z,i}^*\,(1-r_h^{*2})$$

For B_i equal to 1 and the chosen values of ρ_i^* and $V_{z,i}^*$,

$$\psi_t^* = 0.19767$$

which is a constant along the intersecting curve of the stream surface and the casing.

At the inlet station i-i, which is one δ_z-distance upstream of the first station ($z^* = -0.5$), and the exit station e-e, which is one δ_z-distance downstream of the last station ($z^* = 0.85$) (see fig. 2), the radial distribution of ψ^* is computed as follows:

$$\psi_i^*(r) = \psi_e^*(r) = 0.19767\,\frac{r^2-r_h^{\,2}}{r_t^{\,2}-r_h^{\,2}} \tag{27}$$

This simple variation results from the fact that with no tangential and radial velocities of the gas and with uniform values in H and s, the axial velocity and density are also uniform at both these stations. This radial variation in ψ is maintained constant from cycle to cycle and the problem is therefore treated as a boundary-value problem of the first kind.

If the nonhomogeneous term N is everywhere equal to zero, the differential equation (5) would be satisfied by the ψ-function as given by equation (27), which means that the gas flows on cylindrical surfaces. The present problem is then essentially to determine the change of ψ from this simple distribution due to a certain distribution of N in the domain resulting from the nonzero values of density derivatives and F_r. 2402

Calculation of Nonhomogeneous Term

Calculation of density by the use of general table. - The definition of N in the principal equation (5) shows N to consist of two terms for the present investigation. One is connected with the compressibility of the gas, and the other, with the tangential pressure gradient of the gas and the radial twist of the stream surface. The first term in N vanishes for incompressible flow, and its evaluation for compressible flow is as follows:

In each cycle of computation starting with a given variation of ψ, its derivatives with respect to r and z are first obtained by numerical differentiation. These derivatives are squared, added, and used in the following formula to obtain a function Φ

$$\Phi = \left[\left(\frac{\partial\psi^*}{\partial r^*}\right)^2 + \left(\frac{\partial\psi^*}{\partial z^*}\right)^2\right]\left(2H_i^* r^{*2}\right)^{-1}(\rho_{T,i})^{-2}\left(\frac{H}{H_i} - \frac{V_u^{*2}}{2H_i^*}\right)^{-\frac{\gamma+1}{\gamma-1}} \tag{28}$$

The last two factors in the right side of the preceding equation are obtained from the given inlet condition and equation (11). From the value of Φ, a value of Σ is read from table I(b) given in reference 4 (with $\gamma = 4/3$), and ρ^* is obtained by

$$\rho^* = \left(\frac{H}{H_i} - \frac{V_u^{*2}}{2H_i^*}\right)^{\frac{1}{\gamma-1}} \Sigma \tag{29}$$

After ρ^* is evaluated, its derivatives are computed and combined with the ψ-derivatives to form the first term in N.

Calculation of F_r by equation (9) and approximate formulas. - The second term in N involves the use of ρ and $\partial\psi/\partial r$ based on the new values of ψ in each cycle and the evaluation of F_r in the cycle. In order to evaluate F_r, equations (7) to (9) are used. The computation of $F_u r$ by equation (7) is relatively simple (the second term drops out for the present problem). For the computation of F_z of equation (8), the last factor of the last term

2402

$$\left[\frac{\partial^2\psi}{\partial r^2} - \frac{1}{r}\frac{\partial\psi}{\partial r} + \frac{\partial^2\psi}{\partial z^2} - \frac{1}{\rho}\left(\frac{\partial\rho}{\partial r}\frac{\partial\psi}{\partial r} + \frac{\partial\rho}{\partial z}\frac{\partial\psi}{\partial z}\right)\right]$$

is available in the solution by the relaxation method because it is involved in the computation of the residual. In the matrix solution, however, this factor is not available. In such a case, the last term is replaced by the following expression through the use of equation (1):

$$\frac{\partial\psi/\partial z}{\partial\psi/\partial r} F_r$$

in which the value of F_r of the previous cycle is used. After F_z is computed, it is divided by $F_u r$ and differentiated with respect to z. With z_o chosen between two grid points, the formula given in reference 9 is used for the integration to determine F_r.

The following approximate expression for F_r is obtained from equations (7) to (9) by assuming $\partial\psi/\partial r$ constant and neglecting small terms:

$$F_r = \frac{2}{r^3}\frac{\partial(V_u r)}{\partial z}\int_{z_o}^{z}(V_u r)\,dz \tag{30}$$

When equations (14) to (25) are substituted into the preceding equation, the following expressions for dimensionless F_r are obtained:

(a) Uniform loading

Stator: $$F_r^* = \frac{2}{r^{*3}}\left(\frac{0.96}{0.15}\right)^2 \frac{z^{*2}-z_o^{*2}}{2} \tag{31}$$

Rotor: $$F_r^* = -\frac{2}{r^{*3}}\left(\frac{0.96}{0.15}\right)^2 \left[0.35\ (z^*-0.2) - \frac{z^{*2}-0.2^2}{2}\right] \tag{32}$$

(b) Nonuniform loading

Stator: $0 \leq z^* \leq 0.075$,

$$F_r^* = \frac{2}{r^{*3}}\ \frac{4}{3}\ \frac{0.96}{0.15}\left[\frac{4}{3}\ \frac{0.96}{0.15}\ \frac{z^{*2}-z_o^{*2}}{2}\right] \tag{33}$$

$0.075 \leq z^* \leq 0.15$,

$$F_r^* = -\frac{2}{r^{*3}}\ \frac{8}{3}\ \frac{0.96}{0.15}\left(1-\frac{z^*}{0.15}\right)\left[\frac{4}{3}\ \frac{0.96}{0.15}\left(\frac{0.075^2-z_o^{*2}}{2}\right) - 0.32\ (z^*-0.075) + \frac{4}{3}\ \frac{0.96}{0.15}\ (z^{*2}-0.075^2) - \frac{1}{9}\ \frac{z^{*3}-0.075^3}{0.15}\right] \tag{34}$$

Rotor: $0.2 \leq z^* \leq 0.275$,

$$F_r^* = -\frac{2}{r^{*3}}\ \frac{4}{3}\ \frac{0.96}{0.15}\left[0.96(z^*-z_o^*) - \frac{4}{3}\ \frac{0.96}{0.15}\ \frac{(z^*-0.2)^2-(z_o^*-0.2)^2}{2}\right] \tag{35}$$

$0.275 \leq z^* \leq 0.35$,

$$F_r^* = -\frac{2}{r^{*3}}\frac{8}{3}\frac{0.96}{0.15}\left(1-\frac{z^*-0.2}{0.15}\right)\left\{0.96(0.275-z_o^*)-\right.$$

$$\frac{4}{3}\frac{0.96}{0.15}\frac{0.075^2-(z_o^*-0.2)^2}{2}+1.28\,(z^*-z_o^*)\,-$$

$$\frac{4}{3}\frac{0.96}{0.15}\left[(z^*-0.2)^2-(0.075)^2-\right.$$

$$\left.\left.\frac{(z^*-0.2)^3-0.075^3}{3\times 0.15}\right]\right\} \tag{36}$$

Solution of Principal Equation by Relaxation Method

Computation of the residual. - After the nonhomogeneous term N^i is obtained at each grid point, it is subtracted from the left side of equation (26). The difference obtained is the residual at the grid point i.

Reduction of residuals. - The coefficients used to relax residuals (relaxation pattern) are obtained according to the five-point first- and second-order differentiation coefficients in the left side of equation (26). These coefficients for a 0.00001 change in the ψ-value at the grid point are given in table I. These and similar coefficients for other values of change in ψ listed on cards were found to be convenient in calculation. As a combination of checking and time saving, it is found convenient to relax a given set of residuals by using only the central three or five major coefficients at first and, when the residual is small enough, to compute for the total changes in ψ made at each grid point the correct resultant residual everywhere, and then to relax the residuals further with all coefficients. The technique of overrelaxing or underrelaxing and line-relaxing is very helpful. In most cases, the relaxation of 385 points (most relaxation is done in the blade region) is completed within 16 hours by hand computation. The greater portion of work for the present problem is obtaining the residuals, which takes about 40 and 60 hours, by hand computation, for the incompressible and the compressible solutions, respectively. In some of the later relaxation solutions obtained herein, this work of computation of residual is done on the IBM 604 Calculating Punch and an IBM Card Programmed Electronic Calculator (hereinafter called CPEC), except the computation of F_r, which is more difficult to set up. In this way, the calculation of residuals for the compressible flow problem takes about 8 hours of machine time and a few hours of hand computation for F_r.

Solution of Principal Equation by Matrix Method

The 385 simultaneous algebraic equations (26) for the 385 interior grid points can be written in a compact matrix form by denoting the combined coefficients of ψ^j's and ψ^k's in equation (26) at the point i by C^i_j and denoting the sum of N^i and the product of the known boundary ψ-values and their corresponding coefficients by α^i:

$$C^i_j \psi^j = \alpha^i \quad \text{or} \quad [C]\left\{\psi\right\} = \left\{\alpha\right\} \tag{37}$$

The matrix $[C]$ is shown in figure 5 in terms of submatrices $[E]$, $[F]$, and $[G]$. Because there are seven interior grid points in the radial direction, these submatrices are of the order seven, and because of the cylindrical walls and the use of uniform spacing and the same differentiation formula, they repeat regularly along the diagonal of $[C]$. All the other submatrices are zero. The elements of $[E]$, $[F]$, $[G]$ are given in figure 6 in terms of the grid spacings δ_r^* and δ_z^*. In $[F]$ and $[G]$ there are nonzero elements only on the diagonal. With the use of δ_r^* and δ_z^* equal to 0.05 and 0.025, respectively, in order to get the elements of the matrices in short round numbers, the following multiplications are made:

Row of $[C]$	Value of r^*	Multiplication factor
1, 8, 15, ... 379	0.95	0.57
2, 9, 16, ... 380	.90	.54
3, 10, 17, ... 381	.85	.51
4, 11, 18, ... 382	.80	.48
5, 12, 19, ... 383	.75	.45
6, 13, 20, ... 384	.70	.42
7, 14, 21, ... 385	.65	.39

The resultant submatrices are shown in figure 7. The same row multipliers are also applied to the elements of $\left\{\alpha\right\}$ before solving for $\left\{\psi\right\}$.

In the solution of equation (37), because of the aforementioned special nature of $[C]$, it is best to factor $[C]$ into two triangular matrices which also have not more than 15 nonzero elements in a row running alongside the diagonal (references 6, and 10 to 13). Thus

$$[C] = [L][u] \tag{38a}$$

where $[u]$ has elements which are unity along the diagonal, and equation (37) becomes

$$[L][u]\{\psi\} = \{\alpha\} \tag{38b}$$

2702

The solution of $\{\psi\}$ is then obtained by forward and backward substitution processes as follows: Let

$$\{\beta\} = [u]\{\psi\} \tag{39}$$

Then

$$[L]\{\beta\} = \{\alpha\} \tag{40}$$

Solve $\{\beta\}$ from equation (40) and then $\{\psi\}$ from equation (39).

This matrix solution for the present investigation was made on an IBM CPEC and on a UNIVAC. Nine digits are used on the CPEC and eleven digits on the UNIVAC. At no place in the domain do the results obtained for $\{\psi\}$ differ by more than 5 in the sixth digit.

After the solution of $\{\psi\}$ is obtained in each cycle, it is substituted into equation (37) for an over-all check. The residual found at any interior grid point is less than 1 in the eighth digit. Thus, the residual at every interior grid point as found in each cycle of calculation is reduced to practically zero with reference to the accuracy of the grid size chosen. A comparison between the relaxation and the matrix methods showed that more accurate results were obtained with the matrix method in a smaller amount of total man- and machine-hours.

RESULTS AND DISCUSSION

Incompressible Solutions

For adiabatic flow of a nonviscous gas with uniform s and H at the inlet, the deviation of gas flow from that on cylindrical surfaces in the incompressible case is due entirely to the term containing F_r in equation (5). In order to study this effect, solutions are obtained for the two types of loading as given by equations (14) to (21). The one with uniform loading is designated case A, and the one with nonuniform loading, case B.

Convergence of solution. - Similar approaches are used in obtaining the solution for both cases. The calculation for case A is started with an assumption of straight cylindrical flow and successively corrected until the solution converges. The calculation for case B is started from an approximate solution of case A. The initial calculations in both cases are made by the relaxation method with $\delta_r^* = 0.1$ and $\delta_z^* = 0.025$. The values $\delta_r^* = 0.05$ and $\delta_z^* = 0.025$ are used in later calculations. In each cycle, the ψ-values are difficult to improve beyond the fifth decimal place.

The final relaxation solution is further improved by the matrix method. The ψ-values obtained in each matrix solution are resubstituted into equation (26) and the residuals calculated at any point are found to be less than 1 in the eighth decimal place. In the fourth matrix solution all values are sufficiently converged for the grid size and differentiation formula chosen. As an indication of convergence of the solution, the successive values of ψ at the mean radius $r^* = 0.8$ in the matrix solutions of case B are shown in table II. The change in ψ^* in the last cycle is less than 3 in the fifth significant figure or less than 0.003 percent. The variations of ψ^*, $\partial\psi^*/\partial r^*$, $\partial\psi^*/\partial z^*$, $F_u^* r^*$, F_z^*, F_r^*, and N^* at two points $z^* = 0.10$ and 0.25 at the same radius obtained in the matrix solutions as well as the last three relaxation solutions are shown in table III. All results given in the following paragraphs are based on the last matrix solution and are the values on the mean stream surface as indicated in figure 4.

Variation of F components and shape of streamline. - The calculation is first started by using F_r determined by the approximate formula (30). It was later refined by using equations (7) to (9). The variations of $F_u^* r^*$ and F_z^* with z^* at several radii are shown in figures 8(a) and 8(b), respectively. The variation of $F_u^* r^*$ is very similar to that of $\partial(V_u^* r^*)/\partial z^*$ shown in figure 3, being modified only by the variation in V_z^*.

The final values of F_r^* at the same radii are shown in figure 8(c). The starting values determined by the approximate formulas (31) to (36) are also shown in the same figure and are seen to give reasonably good approximate values. The magnitude of F_r is seen to be of the order of a quarter of F_u (figs. 8(a) and 8(c)). This large value of F_r is due to a combination of the large deflection of the gas in passing the turbine blading and the large radial twist of the stream surface of this type of velocity diagram and influences the flow distributions significantly.

2402

Because of this F_r-distribution, the nonhomogeneous term N in equation (5) or (26) is positive upstream of the radial element in the stator and downstream of the radial element in the rotor and is negative between them. The term N also increases in magnitude toward the hub. This distribution of N requires a general increase in ψ at any point inside the blade row from its inlet value at the same radius and results in a streamline shape as shown in figure 9. In both cases A and B, the gas flows radially inward in the stator and outward in the rotor. The difference between the two cases is rather small.

2402

Variation of radial and axial velocities. - The variation of radial velocity with respect to z at several radii is shown in figure 10(a). In both cases A and B, this velocity has a minimum and a maximum about in the middle of the stator and the rotor, respectively. It is practically zero about 1 axial chord upstream and downstream. The radial location of the largest radial velocity occurs around $r^* = 0.75$.

The variation of axial velocity at five radii is shown in figure 10(b). Its deviation from the inlet value is rather large along the casing and the hub, especially in the space between the two blade rows.

Condition in plane normal to turbine axis and between stator and rotor. - In a plane normal to the turbine axis and between the stator and the rotor, the axial velocity is seen to decrease with an increase in the radius (fig. 10(b)). For radially uniform H and s, the equation of motion in the radial direction is

$$\frac{\partial V_r}{\partial z} - \frac{\partial V_z}{\partial r} = F_r$$

Because F_r is zero in the space between the stator and the rotor (fig. 8(c)), the radial velocity must decrease with an increase in z in order to satisfy this equation. This negative slope in V_r with respect to z is clearly shown in case B by the values of radial velocity obtained at the regular grid points at $z^* = 0.15$, 0.175, and 0.20 (fig. 10(a)). For case A, where V_r is nearly equal to zero around $z^* = 0.15$, this negative slope is apparent after the values of V_r at $z^* = 0.1625$ and 0.1875 are computed by using the three-point differentiation formula and the values of ψ at the regular grid points.

It may be noted that this oscillatory variation of velocities in the space between the stator and the rotor is entirely due to the specified variation of $V_u r$ in that space. Because $V_u r$ is specified to

be constant in that space (fig. 4), F_u and F_r on the stream surface are equal to zero in that space according to equations (7) and (9). These values are approached when the number of blades of the stator and rotor approaches infinity. In the actual case of a stream surface between two adjacent blades a finite distance apart, the streamlines turn for a short distance both upstream and downstream of the stator and the rotor (see, for example, reference 7), and consequently, both F_r and the velocities would vary smoothly in the space between the stator and the rotor.

2402

Contours of constant velocity. - A contour plot of constant values of absolute velocity in the stator and relative velocity in the rotor for case B is given in figure 11. The maximum velocities leaving the stator and entering the rotor are, respectively, 1.77 and 1.25 times the rotor tip speed.

Compressible Solution Neglecting F_r

A compressible solution for an inlet Mach number of 0.308 is first obtained by neglecting F_r in the principal equation (case C). This solution is found in order to see the effect of the compressibility term in equation (5) alone and to see the error involved in neglecting F_r for compressible flow. Nonuniform loading is used.

The deviation of flow in this solution from cylindrical flow is due to the density term in N, which is mainly determined by the product $\left(\frac{\partial\rho}{\partial r}\frac{\partial\psi}{\partial r}\right)$. This generally positive value of N inside the stator and the rotor requires a general decrease in ψ at any point inside the stator and the rotor from its inlet value at the same radius, thereby resulting in a streamline shape as shown in figure 12.

In this solution, the starting values for the relaxation solution are obtained by using the values for the gas state at $z^* = 0.175$ obtained in reference 2 and by assuming that the streamline shape varies as a simple sine curve in the meridional plane. The solutions converged quickly. The successive values of ψ^*, $\partial\psi^*/\partial r^*$, $\partial\psi^*/\partial z^*$, ρ^*, and N^* at $r^* = 0.8$ obtained in the matrix and relaxation solutions are given in tables IV and V. The change in ψ^* in the last cycle is less than 2 in the fifth significant figure or about 0.002 percent.

The variations of V_r^*, V_z^*, and ρ^* at several radii obtained in the final matrix solution are shown for case C in figures 13(a), 13(b), and 14, respectively (the curves in those figures for cases D and E will be discussed in the following section). Because of the decrease in density across the turbine, the axial velocity rises to a higher value downstream of the rotor (fig. 13(b)).

Compressible Solutions Including F_r

Solutions are next obtained for compressible flow by considering simultaneously the effects of compressibility and of F_r. As in case C, nonuniform loading is used. Three axial positions of the radial element of the stream surface in the stator ($z_o^* = 0.0625$, 0, and 0.15 for cases D, E, and F, respectively; see fig. 15) are considered in order to investigate the possibility of minimizing the effect of radial flow by the choice of this position. (Conceivably, the stream surface within the stator may have no radial element, its inclination with respect to a radial line being arbitrarily chosen to produce a certain desired effect.) Because of the very large value of F_r and the accompanying large radial flow, the solution for case F was stopped at an early stage, and only the value of F_r obtained in the early relaxation solution and that obtained by the approximate formula (30) are given. The other two cases were carried further by the relaxation method and checked by two to three matrix cycles. Although the solutions are not so far converged as those in cases A, B, and C, they are accurate enough for ordinary purposes. The successive values of ψ and other pertinent variables at a number of typical points for case D are given in tables VI and VII in a manner similar to that for cases B and C.

2402

Nonlinearity of compressible solution. - In the calculation of case D, the values of the later relaxation solutions of case C were used as starting values. The results soon made clear, however, that quicker convergence would have been obtained if the calculation had been started from cylindrical flow. Because of the nonlinear nature of the principal equation, the complete solution for compressible flow for case D cannot be estimated from the solutions obtained in cases B and C. For the two contributions in the nonhomogeneous term N, the first term due to compressibility remains about the same as that in case C, but the second term, containing F_r and ρ, is greatly changed because of the change in density. The distribution of the resultant values of N (and consequently the ψ-distribution) is therefore quite different from that in case B or C or that obtained by directly combining the N-values in the two cases.

Variation of F components. - The variations of $F_u r$, F_z, and F_r are plotted as before in figures 16(a), 16(b), and 16(c), respectively. The variations of $F_u r$ and F_z are similar to those in case B, which has the same type of loading.

A comparison of the F_r-distribution in the stator for the three values of z_o^* chosen shows that alining the stream surface at the stator exit ($z_o^* = 0.15$) causes very large negative values of F_r in

the stator, which will produce large amounts of radial flow. For $z_0^* = 0.0625$, F_r is negative for the first portion and positive for the second portion. For $z_0^* = 0$, F_r is positive everywhere in the stator. The approximate formula (30) for F_r still compared very well with the final values.

Shape of streamline. - The meridional projection of the streamlines obtained for cases D and E is shown in figure 17. In case D, the gas flows radially outward and then inward in the stator, whereas in case E the gas flows radially inward and then outward in the stator. The streamline in case D deviates from a cylindrical surface more than that in case E at the leading edge of the stator but less at the leading edge of the rotor. 2402

Variation of velocities and density. - The variations of V_r and V_z in cases D and E at several radii are shown in figure 13. The radial velocities in these cases are of about the same order of magnitude as the velocity in case C but have more complicated shapes (fig. 13(a)). Figure 13(b) shows that there are significant differences between the values V_z of the three cases C, D, and E, especially at the casing and the hub. These differences are due almost entirely to the different shapes in the streamlines because the differences in density among the three cases are very small (fig. 14).

Contour plots of static pressure and Mach number. - Because of the low value of the hub-tip radius ratio, there is an over-all static-pressure rise across the rotor for values of r^* below 0.7 (fig. 18). An even greater static-pressure rise accompanied by a subsequent reexpansion to the exit pressure occurs within the rotor-blade row; this increase in pressure rise is a result of the flow-area increase associated with the assumption that B is equal to 1.

The contours of constant Mach number (absolute Mach number in stator and relative Mach number in rotor) of cases D and E are shown in figure 19. The maximum Mach numbers at the stator exit are 0.982 and 0.993 for cases D and E, respectively. If the effects of radial flow are completely ignored (simplified radial equilibrium), the maximum Mach number at the stator exit is only 0.927.

Radial variation of axial velocity ahead of rotor. - In the simplified-radial-equilibrium calculation, the axial velocity does not vary radially for free-vortex-type blading. The present solutions show, however, that there is considerable radial variation in axial velocity for both incompressible and compressible flows. An error in the axial velocity of the gas entering a blade row produces an error in Mach number and angle of attack, and thereby the range of efficient

operation is reduced. The radial variation of axial velocity ahead of the rotor (at $z^* = 0.175$) is plotted for cases A to E in figure 20 in which the variation obtained in reference 2 is also plotted for comparison. In all cases except simplified radial equilibrium, the axial velocity decreases with an increase in radius, and the rate of decrease is greatest at the hub. The effect of moving the radial element of the stream surface in the stator from the stator entrance (case E) to the midaxial position in the stator (case D) was to decrease the radial gradient in axial velocity at the rotor entrance. The approximate solution of reference 2 is very close to the solution of case D.

2402

For incompressible flow, this variation is due to the shapes of the streamlines (fig. 9), as influenced by the F_r-distributions (fig. 8(c)), whereas for the compressible flow this variation is due mainly to the increasingly larger drop in density across the stator toward the hub.

SUMMARY OF RESULTS

A method recently developed for determining the steady flow of a nonviscous compressible fluid along a relative stream surface between adjacent blades in a turbomachine was applied to investigate the subsonic through flow in a single-stage axial-flow gas turbine. A free-vortex type of variation in tangential velocity was prescribed along the stream surface. Cylindrical bounding walls were specified in order to avoid radial flow at the walls. The flow variations on the stream surface for incompressible and compressible flows were obtained by using the relaxation method with hand computation and the matrix method on both an IBM Card Programmed Electronic Calculator and a UNIVAC.

In all solutions considered in the present investigation, convergence was obtained without difficulty. A comparison between the relaxation and the matrix methods showed that more accurate results were obtained with the matrix method in a shorter interval of time. The results of these highly accurate through-flow calculations form a basis for evaluation of simpler but less accurate methods.

For incompressible flow, considerable radial flow was obtained because of the circumferential pressure gradient of the gas and the radial twist of the stream surface. The gas flowed radially inward in the stator and radially outward in the rotor. This radial flow resulted in a large negative radial gradient of axial velocity in the space between the stator- and rotor-blade rows.

For compressible flow, the compressibility of the gas and the radial twist of the stream surface had equally important effects on

the flow distribution and the nonlinear behavior of the principal equation defining the flow was quite evident. The shape, or twist, of the stream surface and thus the amount of radial flow were sensitive to the axial location of the radial element of the stream surface in the stator. The largest radial flow occurred when this radial element was located at the exit of the stator. The effect of moving the radial element of the stream surface in the stator from the stator entrance to the midaxial position in the stator was to increase the deviation from cylindrical flow ahead of the stator and to reduce the deviation ahead of the rotor; the radial gradient in axial velocity at the rotor entrance was decreased. When the radial element of the stream surface in the rotor was near the midaxial position in the rotor, a large negative gradient of axial velocity was observed in all cases ahead of the rotor.

2402

Lewis Flight Propulsion Laboratory
National Advisory Committee for Aeronautics
Cleveland, Ohio, April 18, 1952

REFERENCES

1. Eckert and Korbacher: The Flow Through Axial Turbine Stages of Large Radial Length. NACA TM 1118, 1947.

2. Wu, Chung-Hua, and Wolfenstein, Lincoln: Application of Radial-Equilibrium Condition to Axial-Flow Compressor and Turbine Design. NACA Rep. 955, 1950. (Supersedes NACA TN 1795.)

3. Wu, Chung-Hua: A General Through-Flow Theory of Fluid Flow with Subsonic or Supersonic Velocity in Turbomachines of Arbitrary Hub and Casing Shapes. NACA TN 2302, 1951.

4. Wu, Chung-Hua: A General Theory of Three-Dimensional Flow in Subsonic and Supersonic Turbomachines of Axial-, Radial-, and Mixed-Flow Types. NACA TN 2604, 1952.

5. Carter, A. D. S.: Three-dimensional-flow Theories for Axial Compressors and Turbines. War Emergency Issue No. 41, pub. by Inst. Mech. Eng. (London). (Reprinted in U. S. by A.S.M.E., April 1949, pp. 255-268.)

6. Wu, Chung-Hua: Formulas and Tables of Coefficients for Numerical Differentiation with Function Values Given at Unequally Spaced Points and Application to Solution of Partial Differential Equations. NACA TN 2214, 1950.

7. Wu, Chung-Hua, and Brown, Curtis A.: Method of Analysis for Compressible Flow Past Arbitrary Turbomachine Blades on General Surface of Revolution. NACA TN 2407, 1951.

8. Southwell, R. V.: Relaxation Method in Theoretical Physics. Clarendon Press (Oxford), 1946.

9. Lowan, Arnold N., and Salzer, Herbert E.: Table of Coefficients for Numerical Integration Without Differences. Jour. Math. and Physics vol. XXIV, no. 1, Feb. 1945, pp. 1-21.

10. Crout, Prescott D.: A Short Method for Evaluating Determinants and Solving Systems of Linear Equations with Real or Complex Coefficients. AIEE Trans. (Suppl.), vol. 60, 1941, pp. 1235-1241.

11. von Neumann, John, and Goldstine, H. H.: Numerical Inverting of Matrices of High Order. Bull. Am. Math. Soc., vol. 53, no. 11, Nov. 1947, pp. 1021-1099.

12. Turing, A. M.: Round-Off Errors in Matrix Processes. Quart. Jour. Mech. and Appl. Math., vol. 1, 1948, pp. 287-308.

13. Fox, L., Huskey, H. D., and Wilkinson, J. H.: Notes on the Solution of Algebraic Linear Simultaneous Equations. Quart. Jour. Mech. and Appl. Math., vol. 1, 1948, pp. 149-173.

2402

TABLE I - RELAXATION COEFFICIENTS

$\frac{r^i}{r_t}$	For 0.00001 change of ψ at grid point (r^i,z^i), change residual at (r,z) by					
	$\frac{r}{r_t}$	z				
		$z^i - 2\delta_z$	$z^i - \delta_z$	z^i	$z^i + \delta_z$	$z^i + 2\delta_z$
0.95	0.95 .90 .85	-0.00133	0.02133	-0.04684 .00519 -.00031	0.02133	-0.00133
0.90	0.95 .90 .85 .80	-0.00133	0.02133	0.00232 -.05000 .00518 -.00031	0.02133	-0.00133
0.85	0.95 .90 .85 .80 .75	-0.00133	0.02133	0.00123 .00548 -.05000 .00517 -.00031	0.02133	-0.00133
0.80	0.95 .90 .85 .80 .75 .70 .65	-0.00133	0.02133	-0.00032 -.00035 .00549 -.06000 .00516 -.00031 -.00036	0.02133	-0.00133
0.75	0.85 .80 .75 .70 .65	-0.00133	0.02133	-0.00035 .00550 -.05000 .00514 .00149	0.02133	-0.00133
0.70	0.80 .75 .70 .65	-0.00133	0.02133	-0.00035 .00551 -.05000 .00154	0.02133	-0.00133
0.65	0.75 .70 .65	-0.00133	0.02133	-0.00036 .00552 -.04641	0.02133	-0.00133

TABLE II - SUCCESSIVE VALUES OF ψ IN MATRIX SOLUTIONS AT $r^* = 0.8$ FOR CASE B

z^*	Starting value	Matrix solutions				
		First	Second		Third	Fourth
			CPEC	UNIVAC		
-0.500	0.08648	0.086479	0.086478	0.086478	0.086478	0.086478
-.400	.08648	.086475	.086468	.086468	.086468	.086468
-.300	.08648	.086468	.086450	.086450	.086449	.086449
-.200	.08646	.086448	.086415	.086415	.086413	.086412
-.100	.08639	.086395	.086354	.086354	.086350	.086349
-.050	.08636	.086371	.086330	.086330	.086324	.086322
-.025	.08638	.086382	.086333	.086333	.086327	.086325
0	.08647	.086437	.086381	.086381	.086374	.086372
.025	.08695	.086879	.086811	.086811	.086805	.086803
.050	.08775	.087673	.087591	.087591	.087587	.087585
.075	.08882	.088650	.088550	.088550	.088550	.088547
.100	.08976	.089536	.089415	.089415	.089419	.089416
.125	.09042	.090145	.089996	.089996	.090005	.090002
.150	.09086	.090522	.090338	.090338	.090352	.090351
.175	.09139	.090972	.090746	.090746	.090769	.090769
.200	.09187	.091458	.091187	.091187	.091220	.091221
.225	.09152	.091119	.090809	.090810	.090834	.090835
.250	.09073	.090336	.089989	.089989	.090004	.090007
.275	.08982	.089464	.089109	.089107	.089106	.089108
.300	.08908	.088756	.088414	.088414	.088398	.088400
.325	.08858	.088284	.087960	.087960	.087942	.087944
.350	.08824	.087981	.087677	.087677	.087666	.087668
.375	.08794	.087728	.087454	.087454	.087449	.087450
.400	.08765	.087515	.087273	.087273	.087272	.087273
.450	.08723	.087185	.087008	.087008	.087010	.087011
.550	.08676	.086800	.086716	.086716	.086718	.086718
.650	.08656	.086622	.086584	.086584	.086585	.086585
.750	.08649	.086537	.086522	.086522	.086522	.086522
.850	.08648	.086489	.086486	.086486	.086486	.086486

NACA

TABLE III - SUCCESSIVE VALUES OF ψ, $\frac{\partial\psi}{\partial r}$, $\frac{\partial\psi}{\partial z}$, $F_u r$, F_z, F_r, AND N

AT $r^* = 0.8$ FOR CASE B

z^*	Solution	δ_r^*	δ_z^*	ψ^*	$\frac{\partial\psi^*}{\partial r^*}$	$\frac{\partial\psi^*}{\partial z^*}$	$F_u^* r^*$	F_z^*	F_r^*	N^*
0.10	Relaxation	0.10	0.025	0.08987	0.49248	0.03500	3.6851	-7.2194	0.49755	0.58395
		.10	.025	.08982	.49101	.03563	3.6741	-7.2313	.50430	.59364
		.05	.025	.08976	.49217	.03238	3.6828	-7.2353	.51134	.60051
				[a](.08975)						
	Matrix	.05	.025	.0895364	.49377	.03050	3.6948	-7.2374	.51534	.60325
		.05	.025	.0894151	.49266	.02940	3.6865	-7.2386	.51757	.60723
		.05	.025	.0894189	.49270	.02959	3.6867	-7.2380	.51589	.60521
		.05	.025	.0894185	.49269	.02959				
0.25	Relaxation	0.10	0.025	0.09122	0.48654	-0.03647	-5.4610	-1.4682	-0.19868	0.23604
		.10	.025	.09098	.49268	-.03647	-5.5230	-1.4432	-.20870	.24484
		.05	.025	.09073	.49292	-.03603	-5.5327	-1.4453	-.20328	.23837
				[a](.09064)						
	Matrix	.05	.025	.0903360	.49648	-.03527	-5.5726	-1.4367	-.20638	.24837
		.05	.025	.0899893	.49191	-.03599	-5.5213	-1.4371	-.20682	.24302
		.05	.025	.0900044	.49235	-.03667	-5.5263	-1.4376	-.20674	.24271
		.05	.025	.0900065	.49243	-.03665				

[a]Improved value by relaxation method and directly comparable to next value obtained by matrix method.

2402

TABLE IV - SUCCESSIVE VALUES OF ψ IN MATRIX SOLUTIONS AT $r^* = 0.8$ FOR CASE C

z^*	Starting value	Matrix solutions			
		First	Second		Third
			CPEC	UNIVAC	
-0.500	0.08642	0.086475	0.086474	0.086474	0.086474
-.400	.08642	.086451	.086447	.086447	.086448
-.300	.08642	.086399	.086396	.086396	.086396
-.200	.08627	.086285	.086282	.086283	.086283
-.100	.08600	.086024	.086023	.086023	.086023
-.050	.08577	.085789	.085789	.085789	.085788
-.025	.08562	.085631	.085632	.085632	.085631
0	.08543	.085440	.085440	.085441	.085439
.025	.08520	.085211	.085210	.085210	.085210
.050	.08493	.084949	.084947	.084947	.084948
.075	.08467	.084679	.084676	.084676	.084676
.100	.08438	.084439	.084433	.084433	.084434
.125	.08417	.084268	.084258	.084258	.084259
.150	.08414	.084190	.084179	.084180	.084181
.175	.08417	.084218	.084207	.084207	.084208
.200	.08429	.084352	.084342	.084342	.084343
.225	.08454	.084594	.084585	.084585	.084586
.250	.08486	.084884	.084877	.084877	.084878
.275	.08515	.085172	.085166	.085166	.085167
.300	.08541	.085424	.085419	.085419	.085420
.325	.08562	.085630	.085626	.085627	.085627
.350	.08578	.085796	.085793	.085793	.085794
.375	.08591	.085930	.085928	.085928	.085928
.400	.08602	.086040	.086037	.086037	.086037
.450	.08618	.086199	.086195	.086195	.086195
.550	.08628	.086370	.086363	.086363	.086363
.650	.08644	.086437	.086432	.086432	.086433
.750	.08648	.086463	.086462	.086462	.086463
.850	.08648	.086477	.086477	.086477	.086477

NACA

TABLE V - SUCCESSIVE VALUES OF ψ, $\frac{\partial\psi}{\partial r}$, $\frac{\partial\psi}{\partial z}$, ρ, AND N AT $r^* = 0.8$ FOR CASE C

z^*	Solution	δ_r^*	δ_z^*	ψ^*	$\frac{\partial\psi^*}{\partial r^*}$	$\frac{\partial\psi^*}{\partial z^*}$	ρ^*	N^*
0.10	Relaxation	0.05	0.025	0.08442	0.49085	-0.01037	0.82013	0.19948
		.05	.025	.08438	.49592	-.01070	.81871	.20101
	Matrix	.05	.025	.0844393	.49552	-.00840	.81884	.19747
		.05	..025	.0844328	.49602	-.00858	.81870	.19748
		.05	.025	.0844335	.49582	-.00856	.81876	
0.25	Relaxation	0.05	0.025	0.08486	0.49087	0.01253	0.78938	0.06684
		.05	.025	.08486	.49638	.01253	.78771	.06538
	Matrix	.05	.025	.0848845	.49512	.01190	.78810	.06522
		.05	.025	.0848769	.49535	.01191	.78802	.06523
		.05	.025	.0848786	.49528	.01190	.78804	.06550

NACA

2402

TABLE VI - SUCCESSIVE VALUES OF ψ IN MATRIX SOLUTIONS AT $r^* = 0.8$ FOR CASE D

z^*	Starting value	Matrix solutions			
		First		Second	Third
		CPEC	UNIVAC		
-0.500	0.08648	0.086470	0.086470	0.086470	0.086470
-.400	.08642	.086422	.086422	.086419	.086420
-.300	.08628	.086330	.086330	.086324	.086324
-.200	.08597	.086123	.086123	.086114	.086114
-.100	.08539	.085657	.085657	.085653	.085651
-.050	.08497	.085264	.085264	.085265	.085262
-.025	.08474	.085020	.085021	.085026	.085023
0	.08452	.084773	.084773	.084782	.084778
.025	.08466	.084860	.084861	.084872	.084868
.050	.08511	.085238	.085239	.085254	.085249
.075	.08568	.085730	.085731	.085753	.085747
.100	.08614	.086114	.086114	.086148	.086140
.125	.08641	.086312	.086312	.086358	.086350
.150	.08660	.086433	.086433	.086492	.086483
.175	.08694	.086713	.086713	.086785	.086775
.200	.08741	.087137	.087137	.087219	.087207
.225	.08744	.087124	.087124	.087220	.087206
.250	.08720	.086859	.086859	.086971	.086953
.275	.08691	.086558	.086558	.086682	.086661
.300	.08671	.086361	.086361	.086498	.086474
.325	.08662	.086313	.086313	.086432	.086407
.350	.08659	.086331	.086331	.086433	.086409
.375	.08656	.086352	.086353	.086440	.086417
.400	.08653	.086373	.086373	.086448	.086426
.450	.08650	.086406	.086406	.086461	.086443
.550	.08647	.086447	.086447	.086474	.086464
.650	.08648	.086465	.086465	.086479	.086473
.750	.08648	.086474	.086474	.086480	.086477
.850	.08648	.086479	.086479	.086480	.086479

NACA

TABLE VII - SUCCESSIVE VALUES OF ψ, $\frac{\partial\psi}{\partial r}$, $\frac{\partial\psi}{\partial z}$, ρ, AND N AT $r^* = 0.8$ FOR CASE D

z^*	Solution	δ_r^*	δ_z^*	ψ^*	$\frac{\partial\psi^*}{\partial r^*}$	$\frac{\partial\psi^*}{\partial z^*}$	ρ^*	F_r^*	N^*
0.10	Relaxation	0.10	0.025	0.08616	0.49474	0.00888	0.81905	0.52876	-0.28438
		.10	.025	.08609	.49661	.01593	.81847	.54071	-.31213
		.05	.025	.08615	.49675	.01393	.81845	.54193	-.30862
		.05	.025	.08614	.49612	.01450	.81863	.53724	-.30484
				[a](.08614)					
	Matrix	.05	.025	.086114	.49530	.011534	.81889	.54006	-.30277
		.05	.025	.086148	.49567	.012020	.81878	.53905	-.30187
		.05	.025	.086140	.49564	.011969	.81879		
0.25	Relaxation	0.10	0.025	0.08737	0.49501	-0.00562	0.78815	0.20438	-0.06956
		.10	.025	.08726	.49521	-.01177	.78807	.20388	-.06909
		.05	.025	.08720	.49493	-.01180	.78815	.20419	-.06843
		.05	.025	.08720	.49573	-.01180	.78791	.20740	-.06732
				[a](.08718)					
	Matrix	.05	.025	.086859	.49450	-.012527	.78827	.20320	-.06944
		.05	.025	.086971	.49483	-.011951	.78818	.20331	-.06983
		.05	.025	.086953	.49488	-.012092	.78816		

[a]Improved value by relaxation method and directly comparable to next value obtained by matrix method.

2402

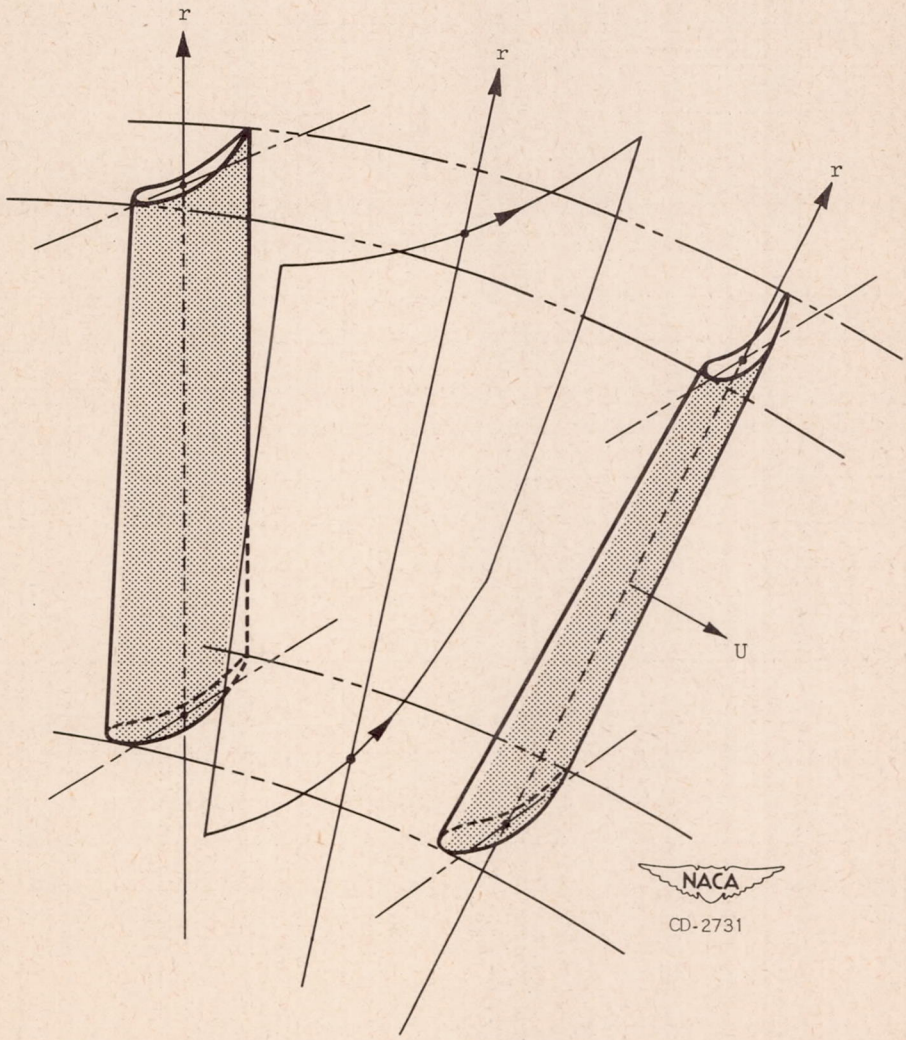

Figure 1. Relative stream surface about midway between adjacent blades.

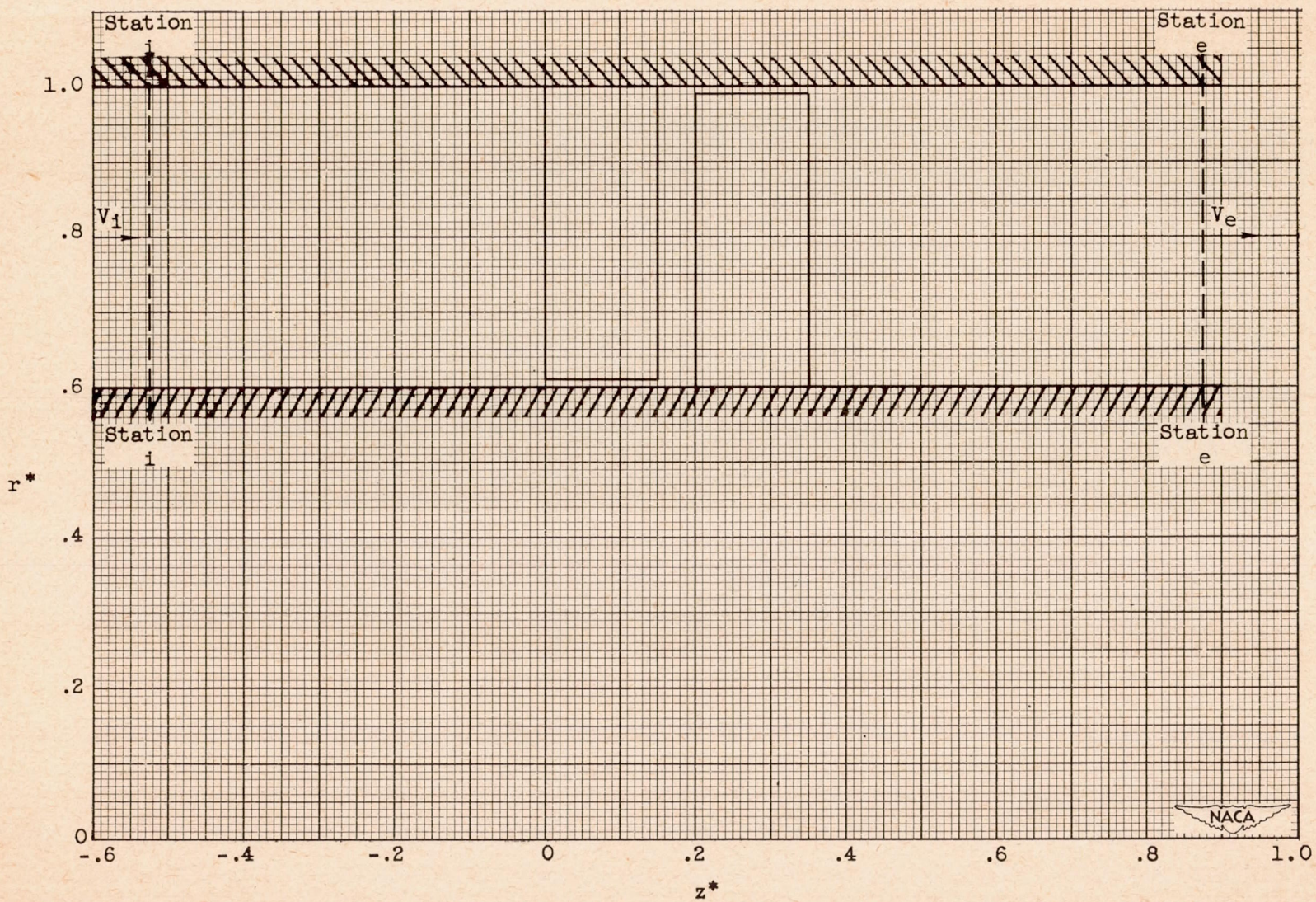

Figure 2. - Meridional section of gas turbine.

2402

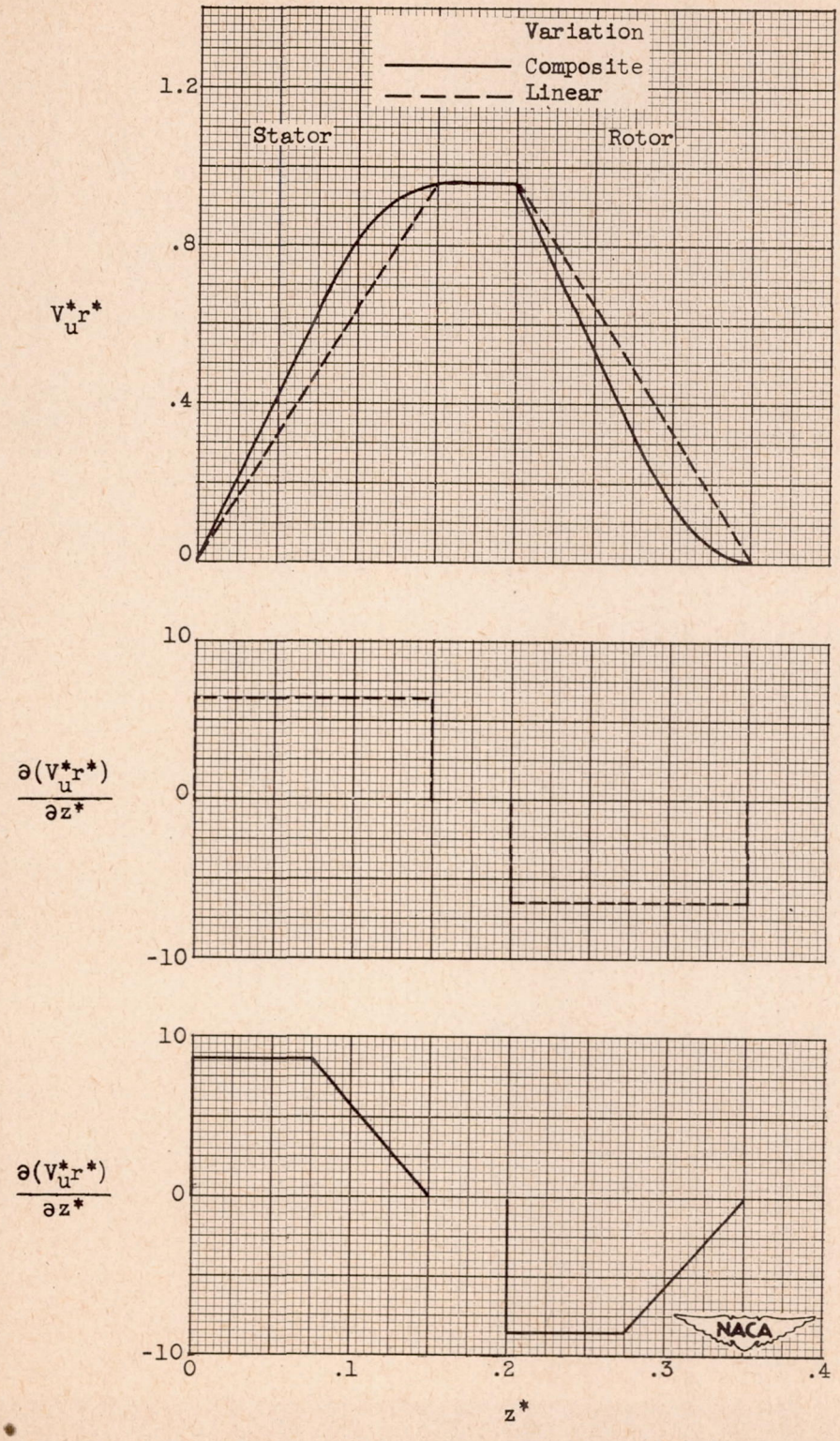

Figure 3. - Specified variation of tangential velocity $V_u^* r^*$ with respect to axial distance z^*.

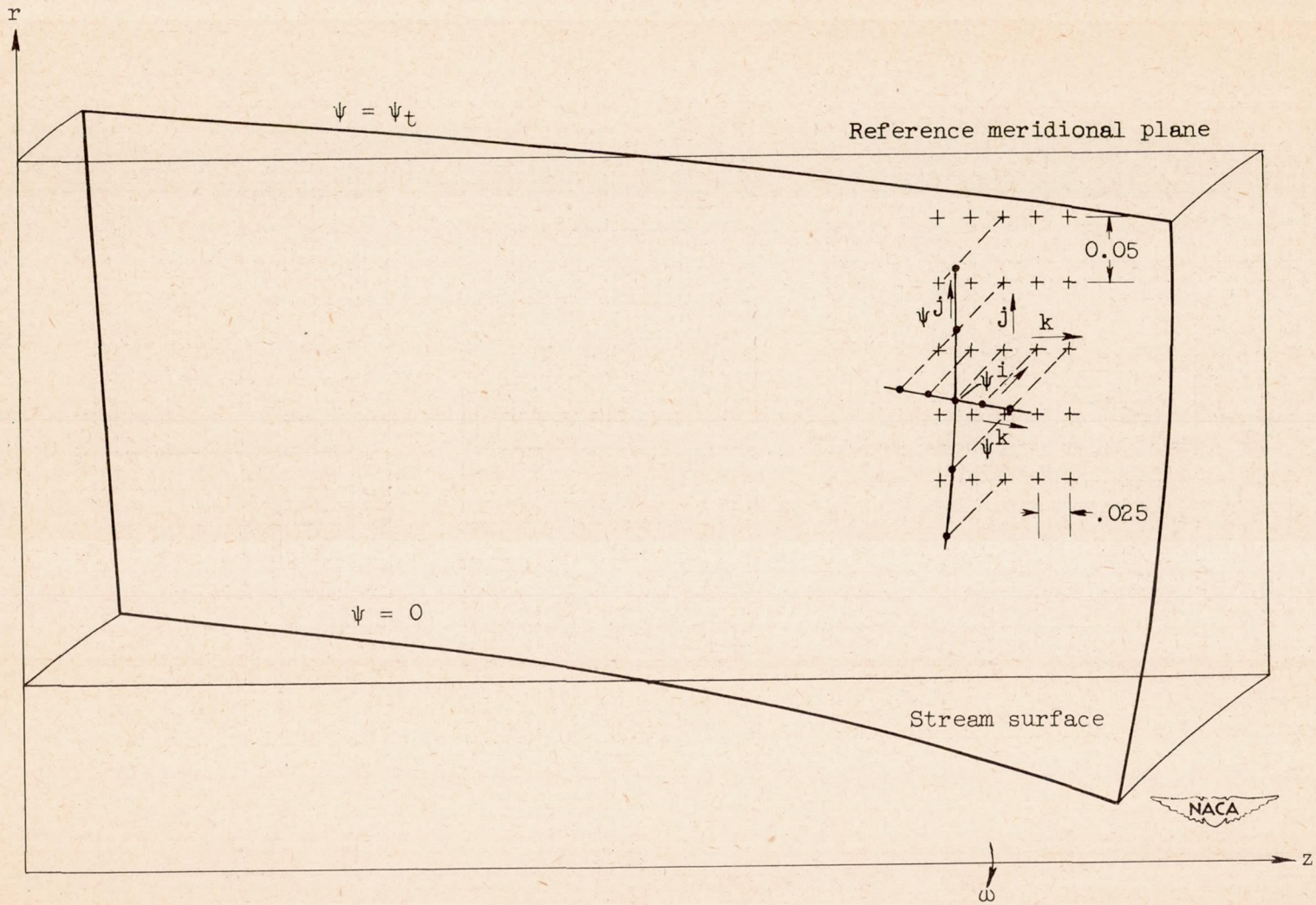

Figure 4. - Grid system and relation between stream surface and reference meridional plane.

2402

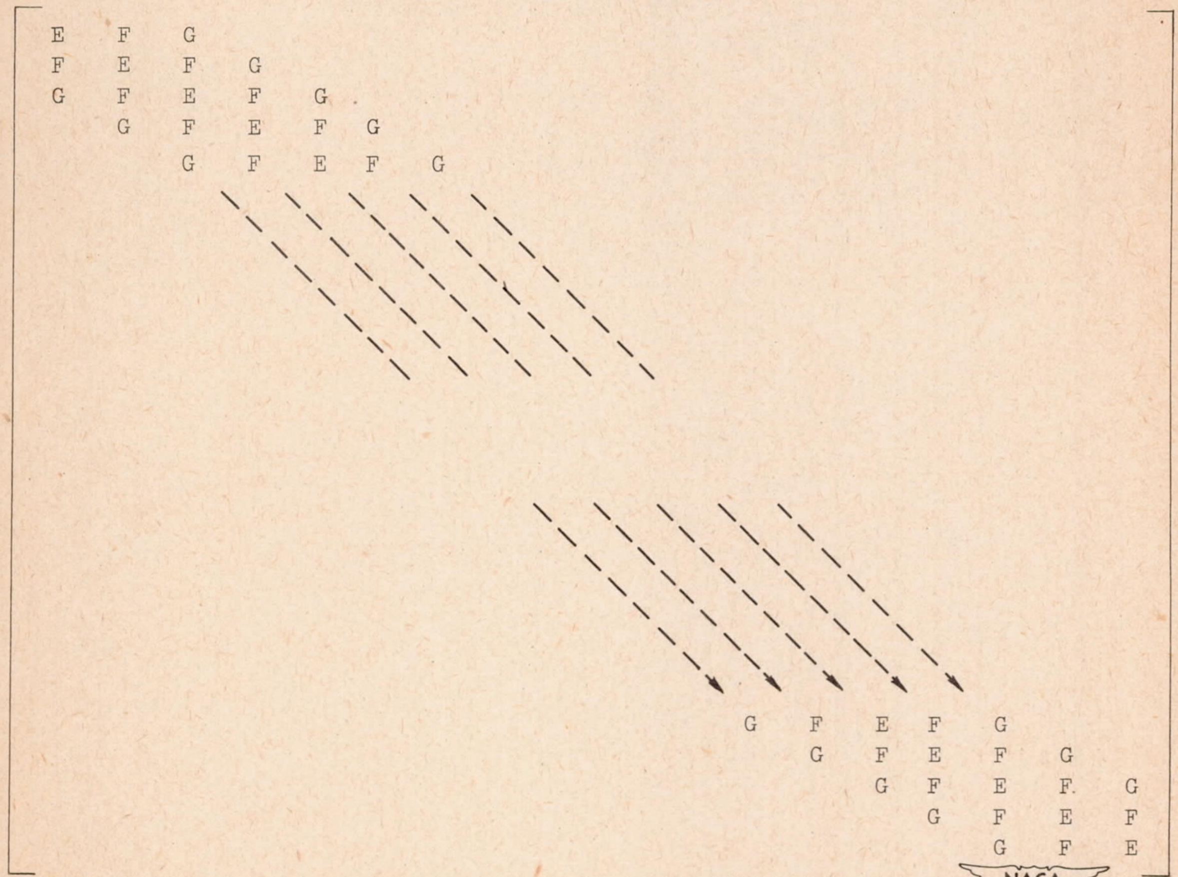

Figure 5. - Matrix [C] expressed in terms of submatrices [E], [F], and [G].

$$
\begin{bmatrix}
-\frac{5}{3a^2}-\frac{5}{0.95\times 6a}-\frac{5}{2b^2} & \frac{1}{2a^2}+\frac{3}{0.95\times 2a} & \frac{1}{3a^2}-\frac{1}{0.95\times 2a} & -\frac{1}{12a^2}+\frac{1}{0.95\times 12a} & 0 & 0 & 0 \\
\frac{4}{3a^2}-\frac{2}{0.9\times 3a} & -\frac{30}{12a^2}-\frac{5}{2b^2} & \frac{4}{3a^2}+\frac{2}{0.9\times 3a} & -\frac{1}{12a^2}-\frac{1}{0.9\times 12a} & 0 & 0 & 0 \\
-\frac{1}{12a^2}+\frac{1}{0.85\times 12a} & \frac{4}{3a^2}-\frac{2}{0.85\times 3a} & -\frac{30}{12a^2}-\frac{5}{2b^2} & \frac{4}{3a^2}+\frac{2}{0.85\times 3a} & -\frac{1}{12a^2}-\frac{1}{0.85\times 12a} & 0 & 0 \\
0 & -\frac{1}{12a^2}+\frac{1}{0.8\times 12a} & \frac{4}{3a^2}-\frac{2}{0.8\times 3a} & -\frac{30}{12a^2}-\frac{5}{2b^2} & \frac{4}{3a^2}+\frac{2}{0.8\times 3a} & -\frac{1}{12a^2}-\frac{1}{0.8\times 12a} & 0 \\
0 & 0 & -\frac{1}{12a^2}+\frac{1}{0.75\times 12a} & \frac{4}{3a^2}-\frac{2}{0.75\times 3a} & -\frac{30}{12a^2}-\frac{5}{2b^2} & \frac{4}{3a^2}+\frac{2}{0.75\times 3a} & -\frac{1}{12a^2}-\frac{1}{0.75\times 12a} \\
0 & 0 & 0 & -\frac{1}{12a^2}+\frac{1}{0.7\times 12a} & \frac{4}{3a^2}-\frac{2}{0.7\times 3a} & -\frac{30}{12a^2}-\frac{5}{2b^2} & \frac{4}{3a^2}+\frac{2}{0.7\times 3a} \\
0 & 0 & 0 & -\frac{1}{12a^2}+\frac{1}{0.65\times 12a} & \frac{1}{3a^2}+\frac{1}{0.65\times 2a} & \frac{1}{2a^2}-\frac{3}{0.65\times 2a} & -\frac{5}{3a^2}+\frac{5}{0.65\times 6a}-\frac{5}{2b^2}
\end{bmatrix}
$$

(a) Submatrix [E].

Figure 6. - Submatrices [E], [F], and [G] expressed in terms of grid spacings δ_r^* and δ_z^*. $a = \delta_r^*$; $b = \delta_z^*$.

2402

$$\begin{bmatrix} \frac{16}{12b^2} & 0 & 0 & 0 & 0 & 0 & 0 \\ 0 & \frac{16}{12b^2} & 0 & 0 & 0 & 0 & 0 \\ 0 & 0 & \frac{16}{12b^2} & 0 & 0 & 0 & 0 \\ 0 & 0 & 0 & \frac{16}{12b^2} & 0 & 0 & 0 \\ 0 & 0 & 0 & 0 & \frac{16}{12b^2} & 0 & 0 \\ 0 & 0 & 0 & 0 & 0 & \frac{16}{12b^2} & 0 \\ 0 & 0 & 0 & 0 & 0 & 0 & \frac{16}{12b^2} \end{bmatrix}$$

(b) Submatrix [F].

$$\begin{bmatrix} -\frac{1}{12b^2} & 0 & 0 & 0 & 0 & 0 & 0 \\ 0 & -\frac{1}{12b^2} & 0 & 0 & 0 & 0 & 0 \\ 0 & 0 & -\frac{1}{12b^2} & 0 & 0 & 0 & 0 \\ 0 & 0 & 0 & -\frac{1}{12b^2} & 0 & 0 & 0 \\ 0 & 0 & 0 & 0 & -\frac{1}{12b^2} & 0 & 0 \\ 0 & 0 & 0 & 0 & 0 & -\frac{1}{12b^2} & 0 \\ 0 & 0 & 0 & 0 & 0 & 0 & -\frac{1}{12b^2} \end{bmatrix}$$

(c) Submatrix [G].

Figure 6. - Concluded. Submatrices [E], [F], and [G] expressed in terms of grid spacings δ_r^* and δ_z^*. $a = \delta_r^*$; $b = \delta_z^*$.

2402

$$\begin{bmatrix} -2670 & 132 & 70 & -18 & 0 & 0 & 0 \\ 280 & -2700 & 296 & -19 & 0 & 0 & 0 \\ -16 & 264 & -2550 & 280 & -18 & 0 & 0 \\ 0 & -15 & 248 & -2400 & 264 & -17 & 0 \\ 0 & 0 & -14 & 232 & -2250 & 248 & -16 \\ 0 & 0 & 0 & -13 & 216 & -2100 & 232 \\ 0 & 0 & 0 & -14 & 58 & 60 & -1810 \end{bmatrix}$$

(a) Submatrix [E].

$$\begin{bmatrix} 1216 & 0 & 0 & 0 & 0 & 0 & 0 \\ 0 & 1152 & 0 & 0 & 0 & 0 & 0 \\ 0 & 0 & 1088 & 0 & 0 & 0 & 0 \\ 0 & 0 & 0 & 1024 & 0 & 0 & 0 \\ 0 & 0 & 0 & 0 & 960 & 0 & 0 \\ 0 & 0 & 0 & 0 & 0 & 896 & 0 \\ 0 & 0 & 0 & 0 & 0 & 0 & 832 \end{bmatrix}$$

(b) Submatrix [F].

$$\begin{bmatrix} -76 & 0 & 0 & 0 & 0 & 0 & 0 \\ 0 & -72 & 0 & 0 & 0 & 0 & 0 \\ 0 & 0 & -68 & 0 & 0 & 0 & 0 \\ 0 & 0 & 0 & -64 & 0 & 0 & 0 \\ 0 & 0 & 0 & 0 & -60 & 0 & 0 \\ 0 & 0 & 0 & 0 & 0 & -56 & 0 \\ 0 & 0 & 0 & 0 & 0 & 0 & -52 \end{bmatrix}$$

(c) Submatrix [G].

Figure 7. - Submatrices [E], [F], and [G] after row multiplication.

2402

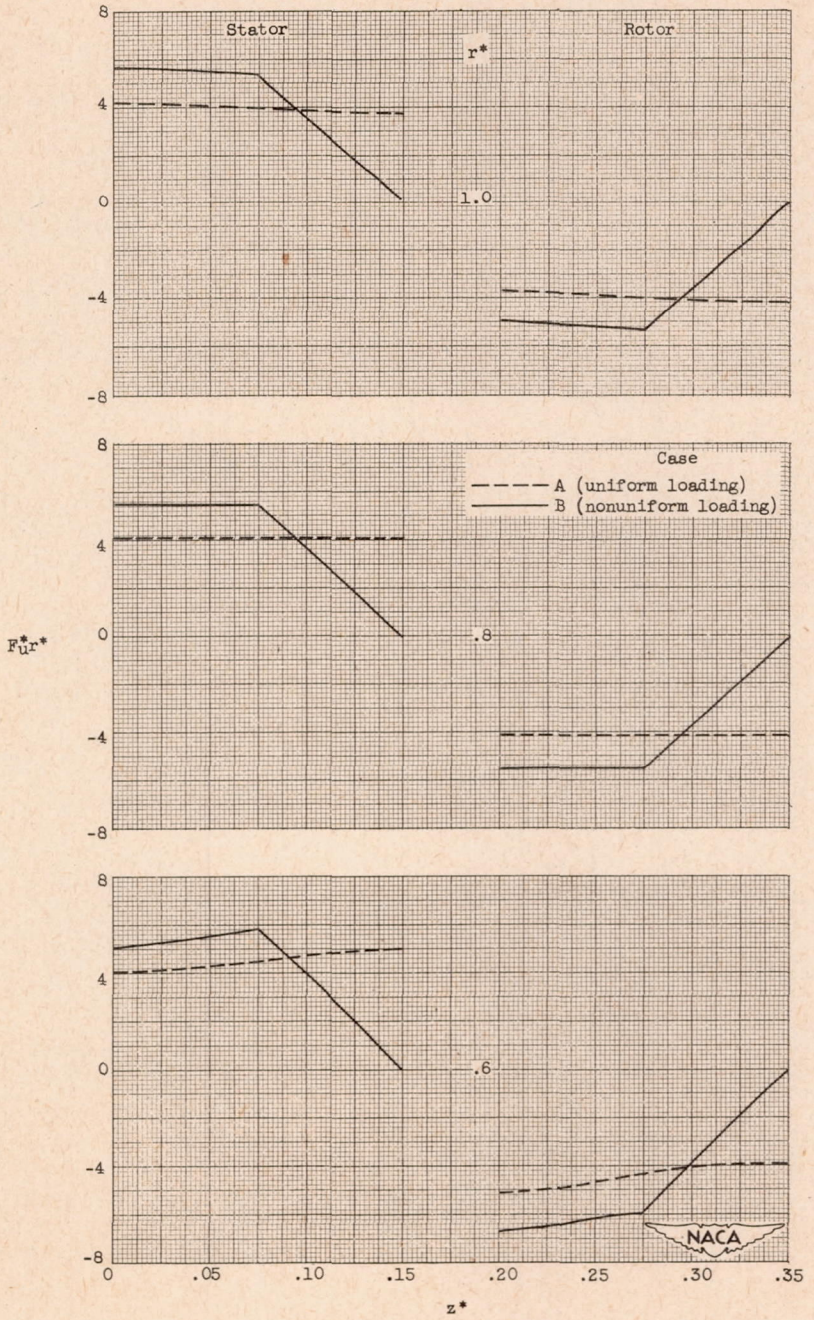

(a) $F_{ur^*}^*$.

Figure 8. - Variation of F in incompressible solutions.

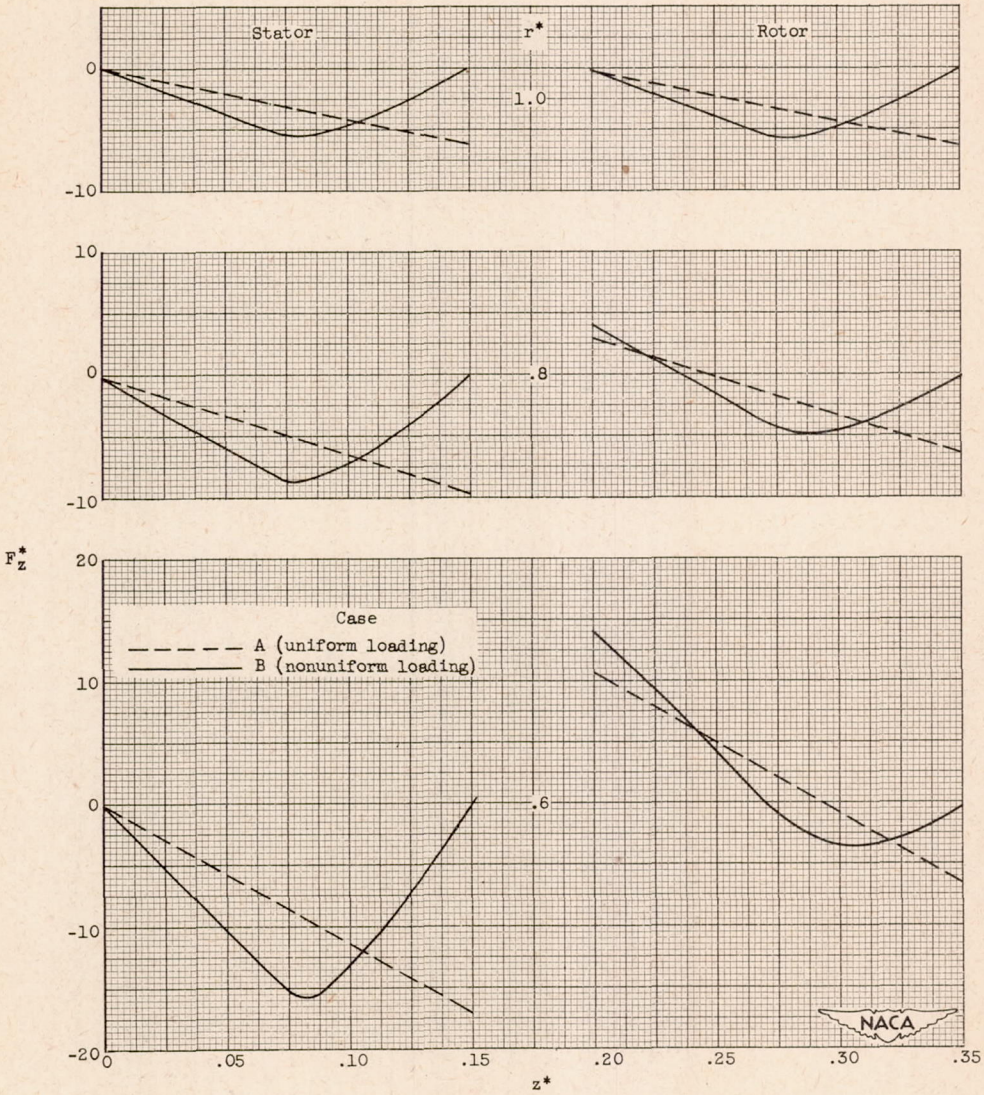

(b) F_z^*.

Figure 8. - Continued. Variation of F in incompressible solutions.

2402

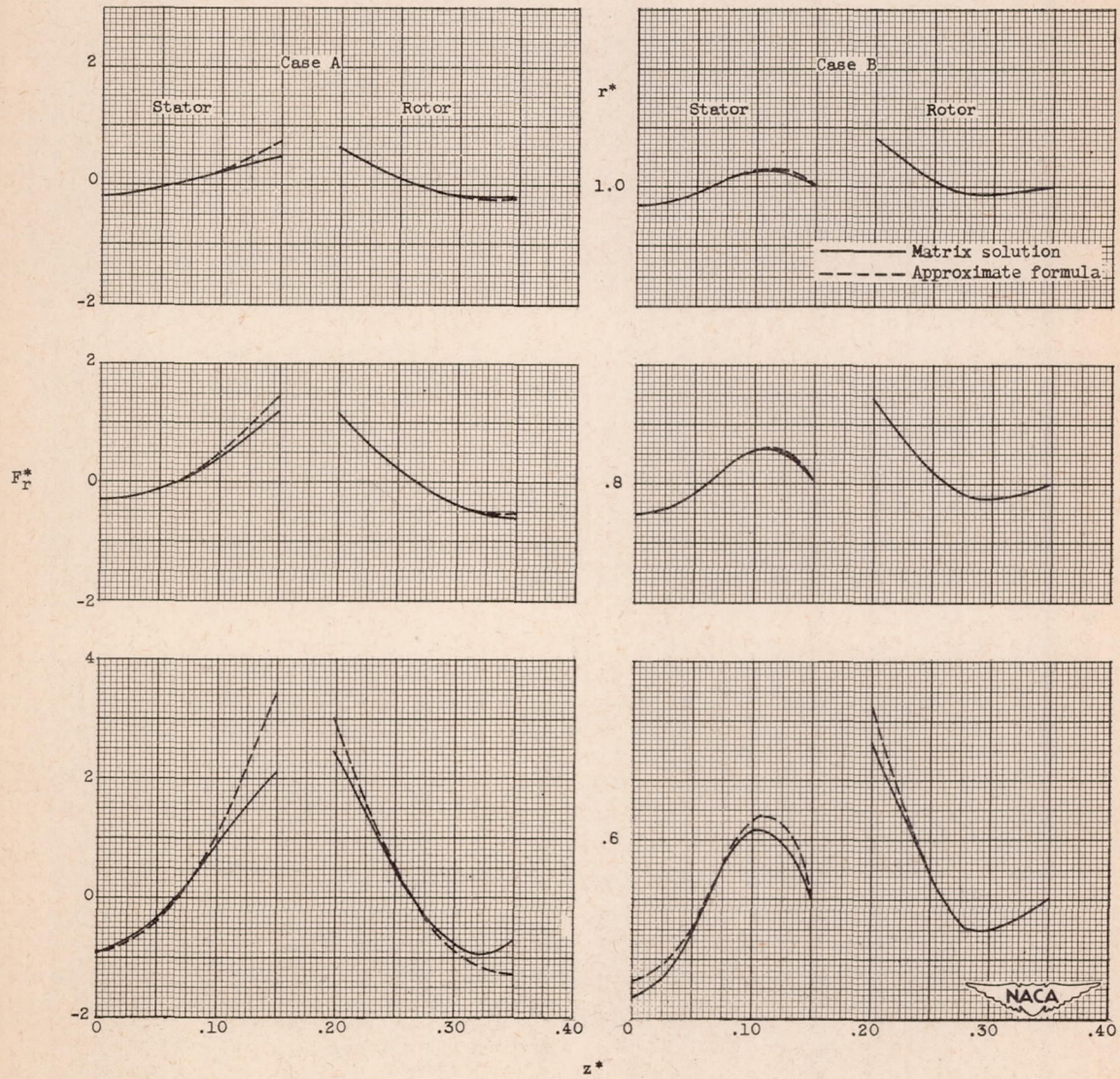

(c) F_r^*.

Figure 8. - Concluded. Variation of F in incompressible solutions.

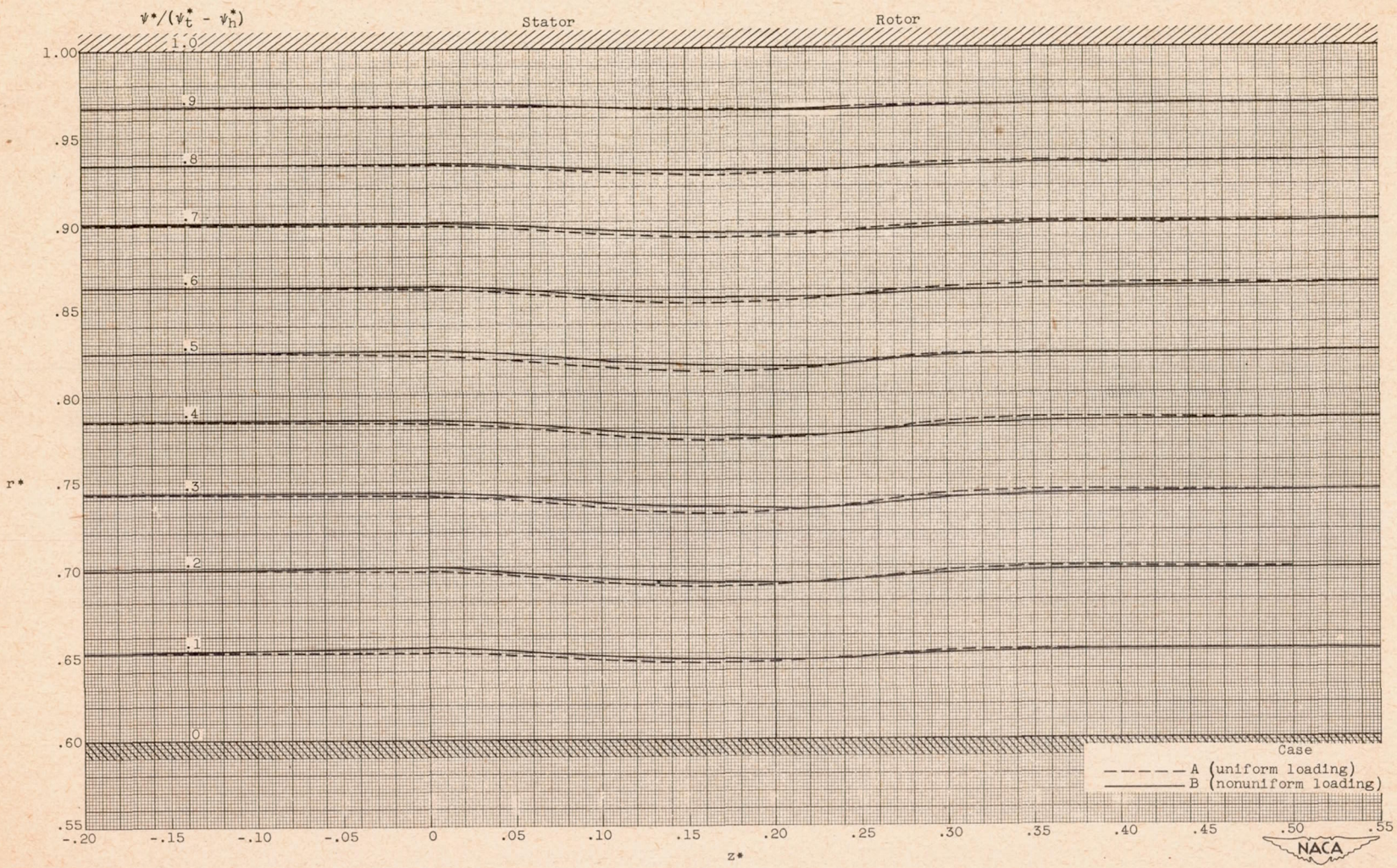

Figure 9. - Meridional projection of streamlines of incompressible solutions.

2402

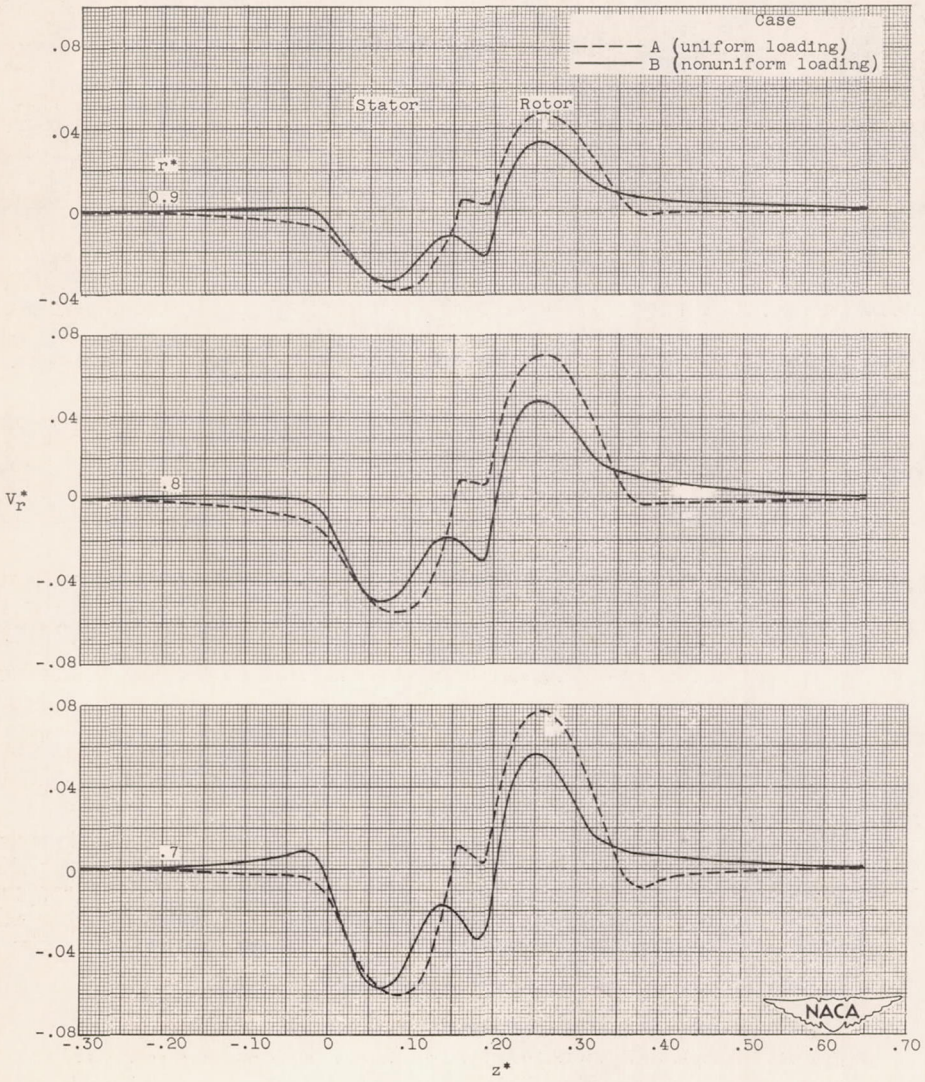

(a) Radial velocity V_r^*.

Figure 10. - Variation of velocities in incompressible solutions.

2402

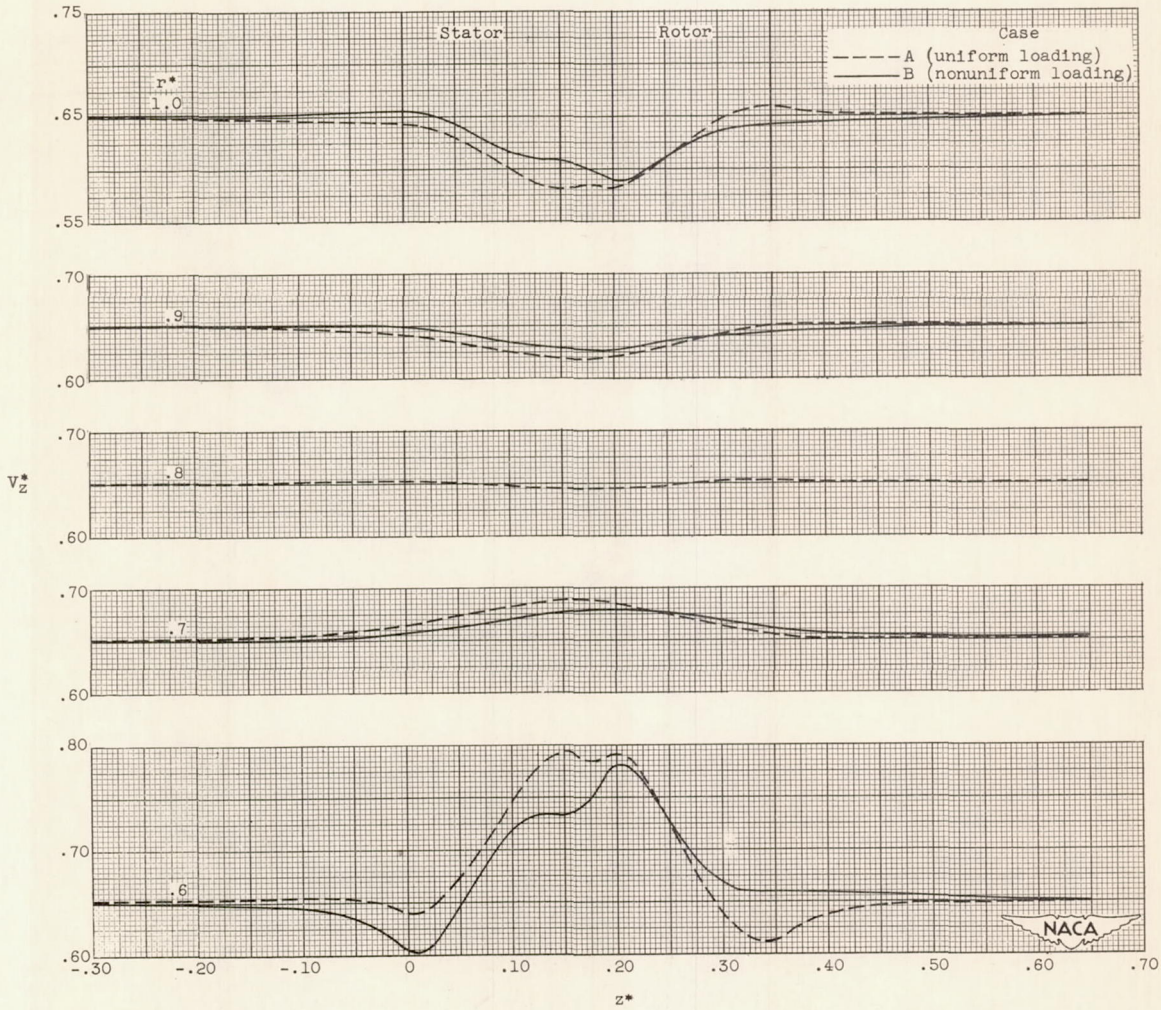

(b) Axial velocity V_z^*.

Figure 10. - Concluded. Variation of velocities in incompressible solutions.

2402

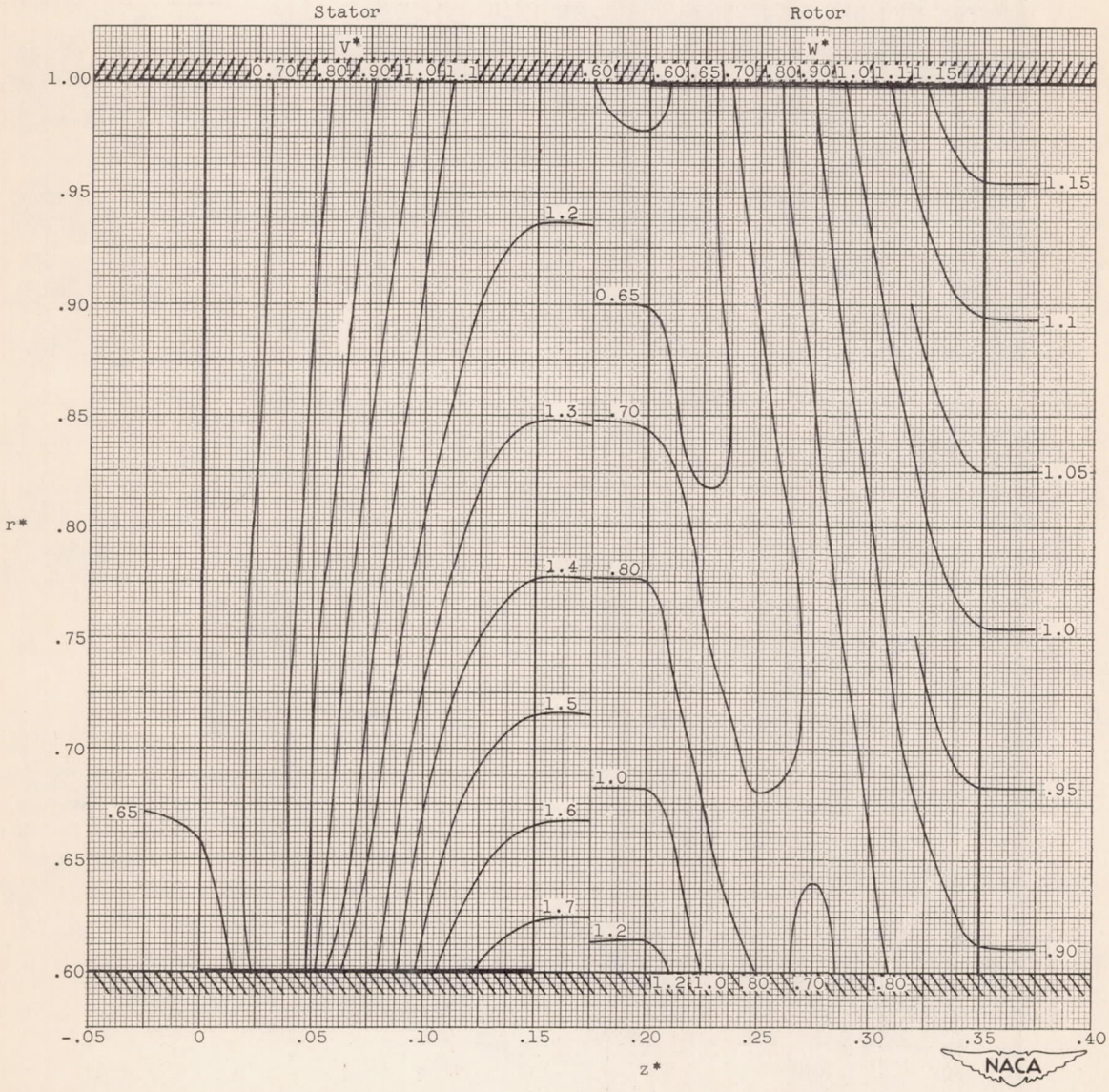

Figure 11. - Contours of constant absolute velocity in stator and relative velocity in rotor in case B.

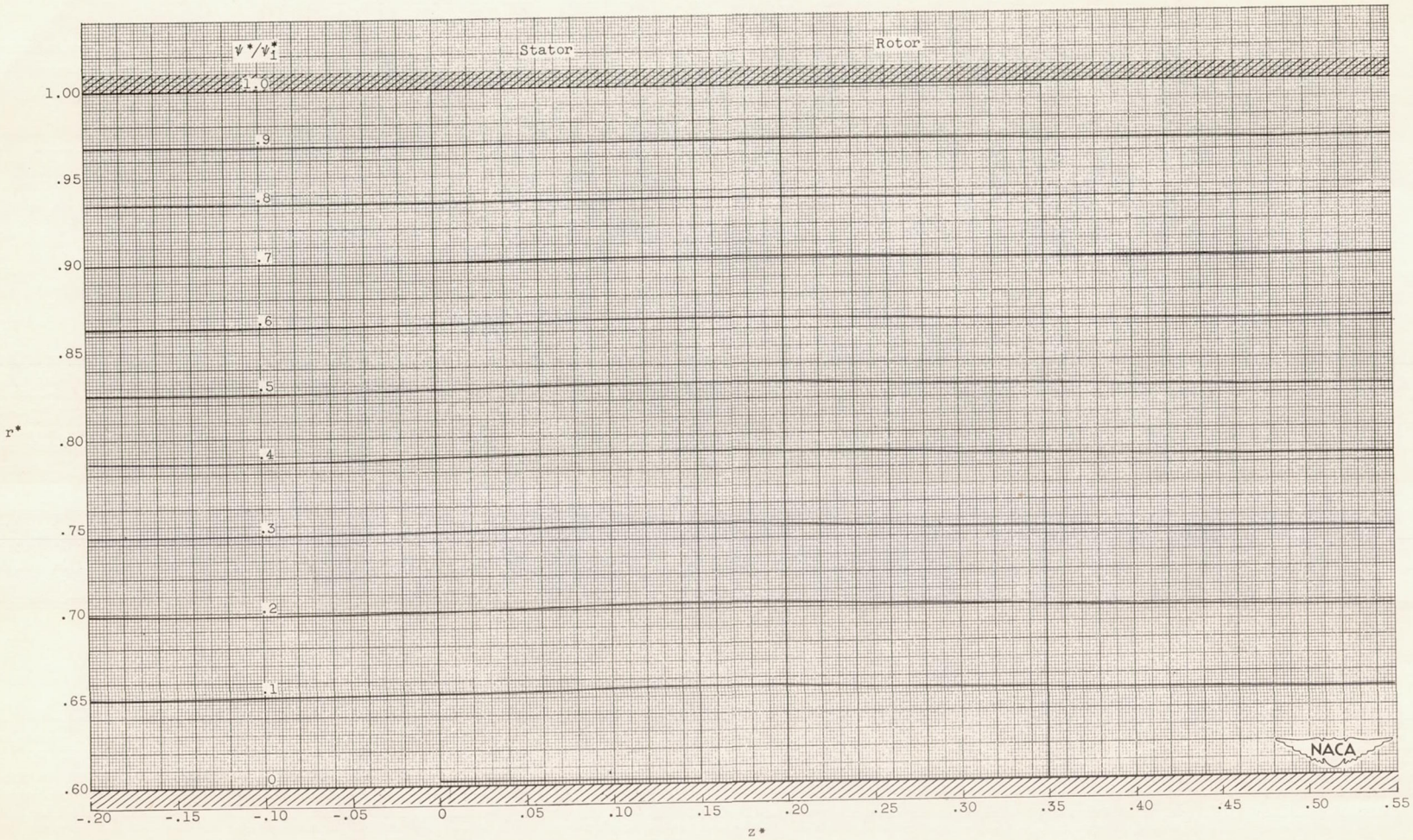

Figure 12. - Meridional projection of streamlines for compressible solution neglecting F_r.

2402

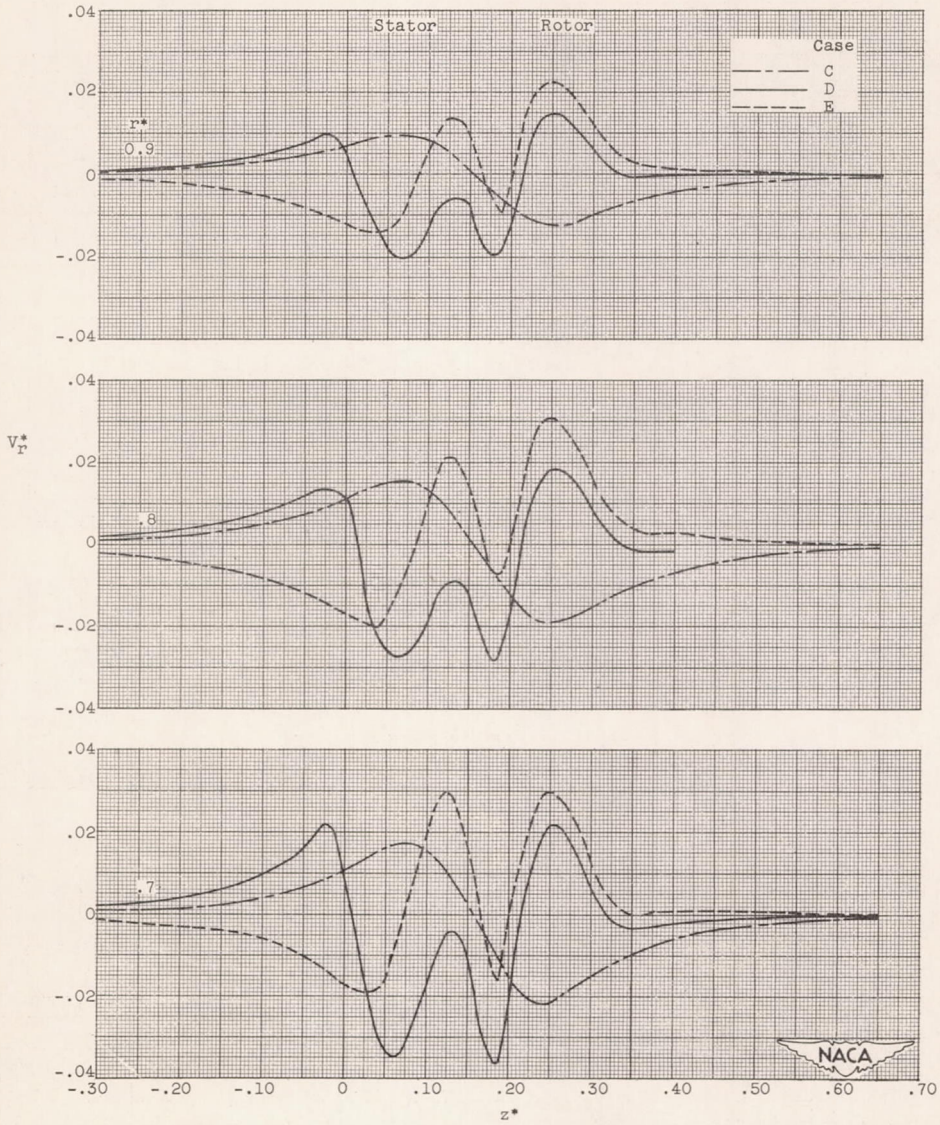

(a) Radial velocity V_r^*.

Figure 13. - Variation of velocities in compressible solutions.

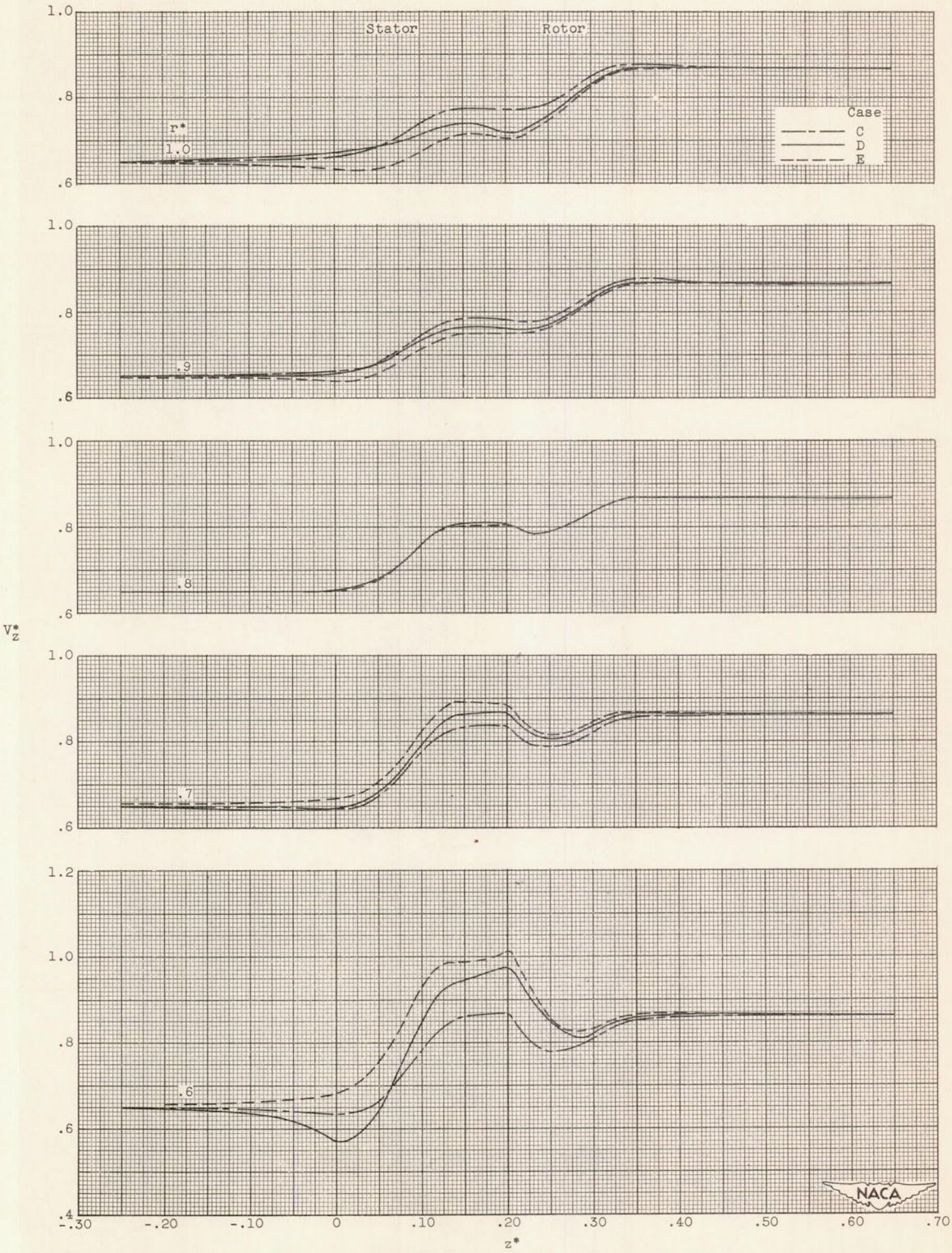

(b) Axial velocity V_z^*.

Figure 13. - Concluded. Variation of velocities in compressible solutions.

2402

2402

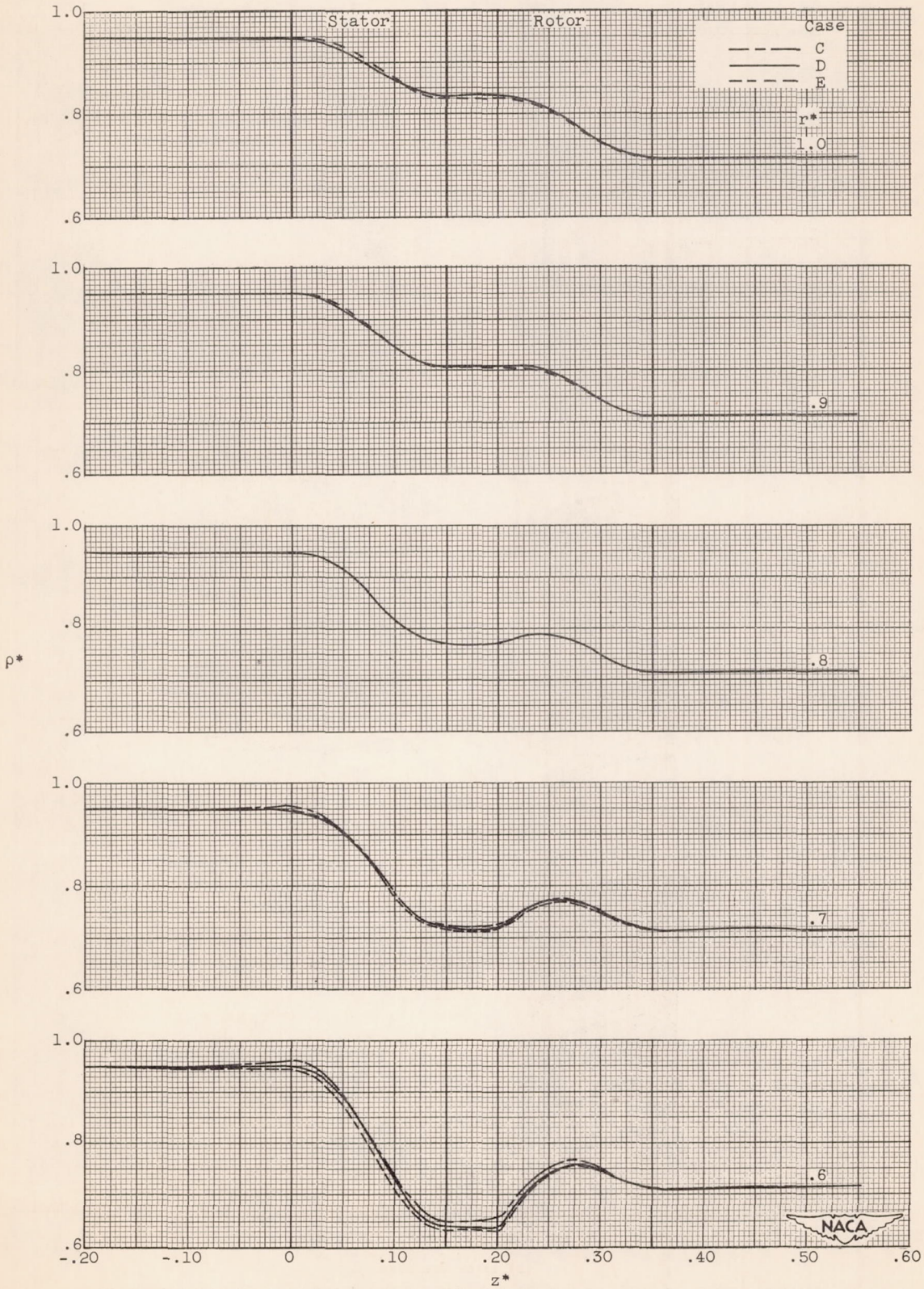

Figure 14. - Variation of density in compressible solutions.

2402

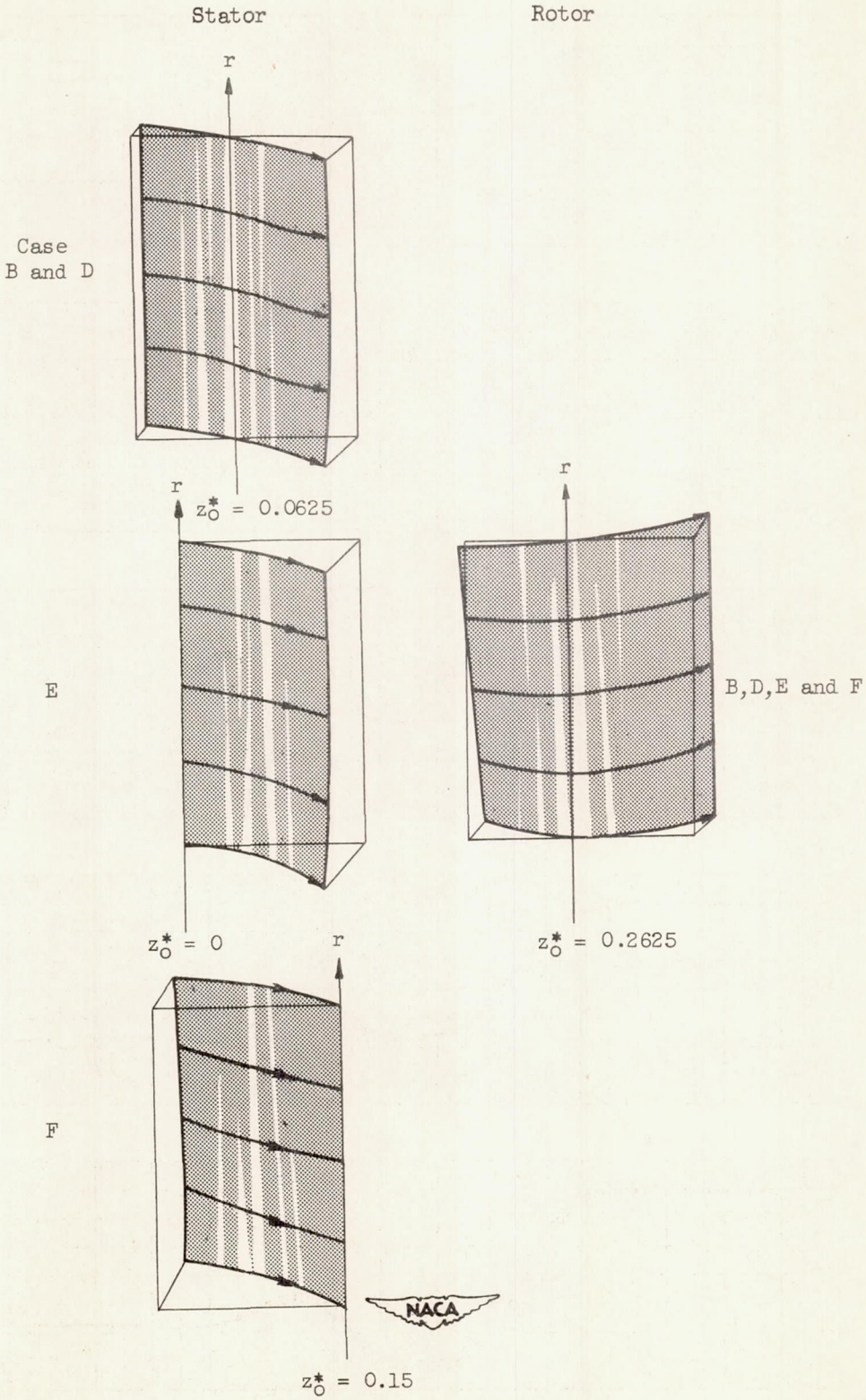

Figure 15. - Axial position of radial element of stream surfaces.

2402

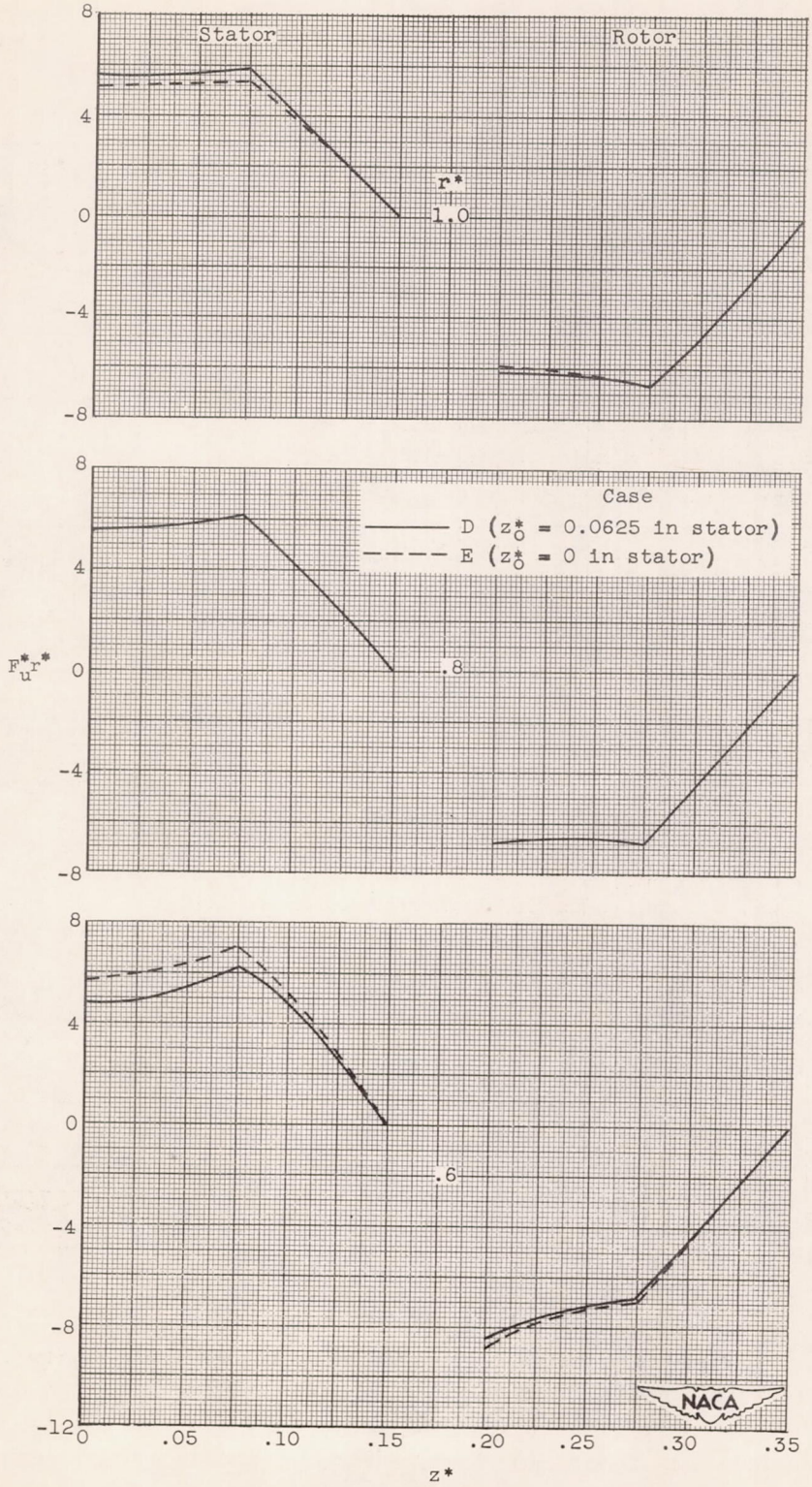

(a) $F_u^* r^*$ for cases D and E.

Figure 16. - Variation of F in compressible solutions.

2402

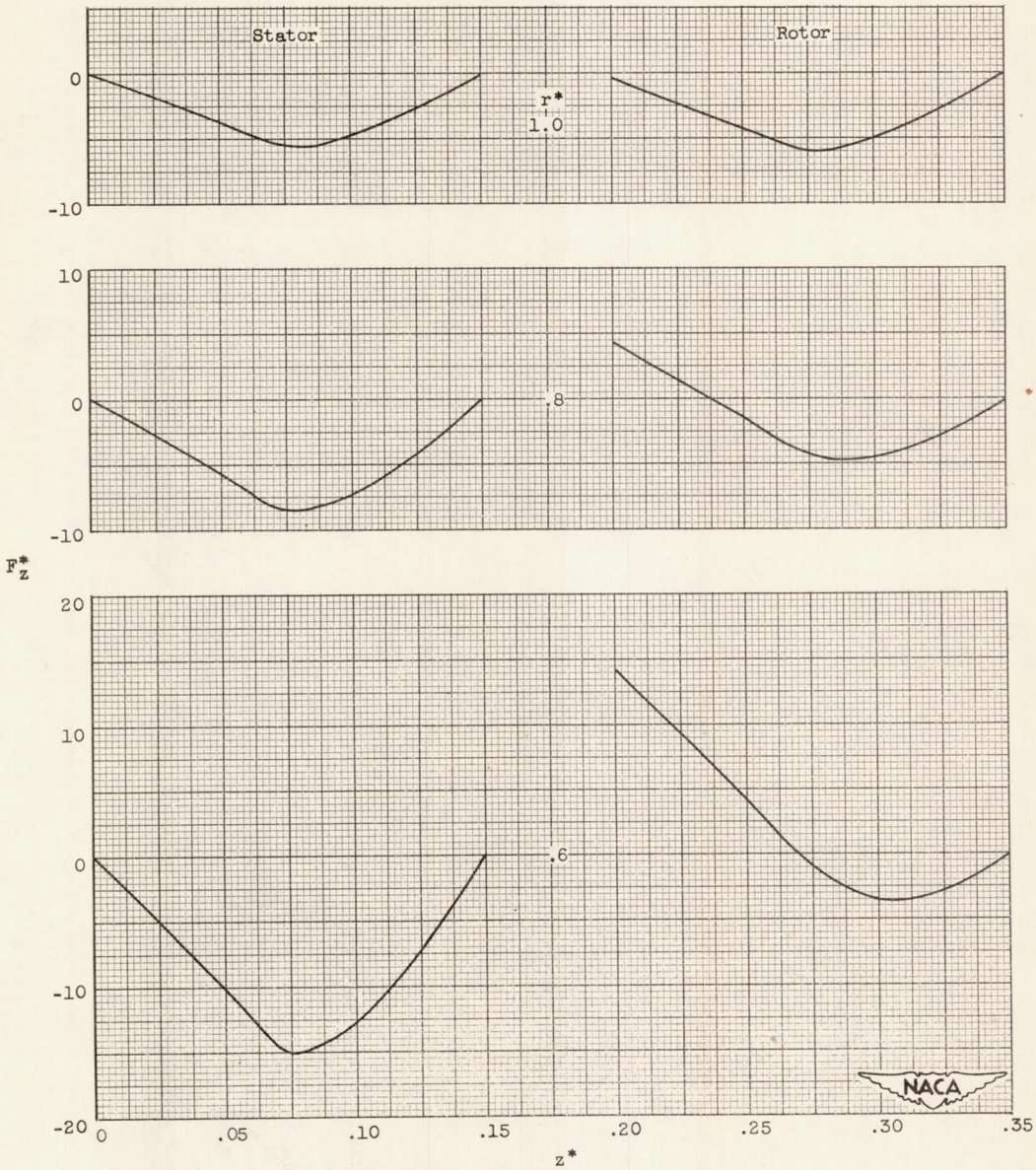

(b) F_z^* for cases D and E.

Figure 16. - Continued. Variation of F in compressible solutions.

2402

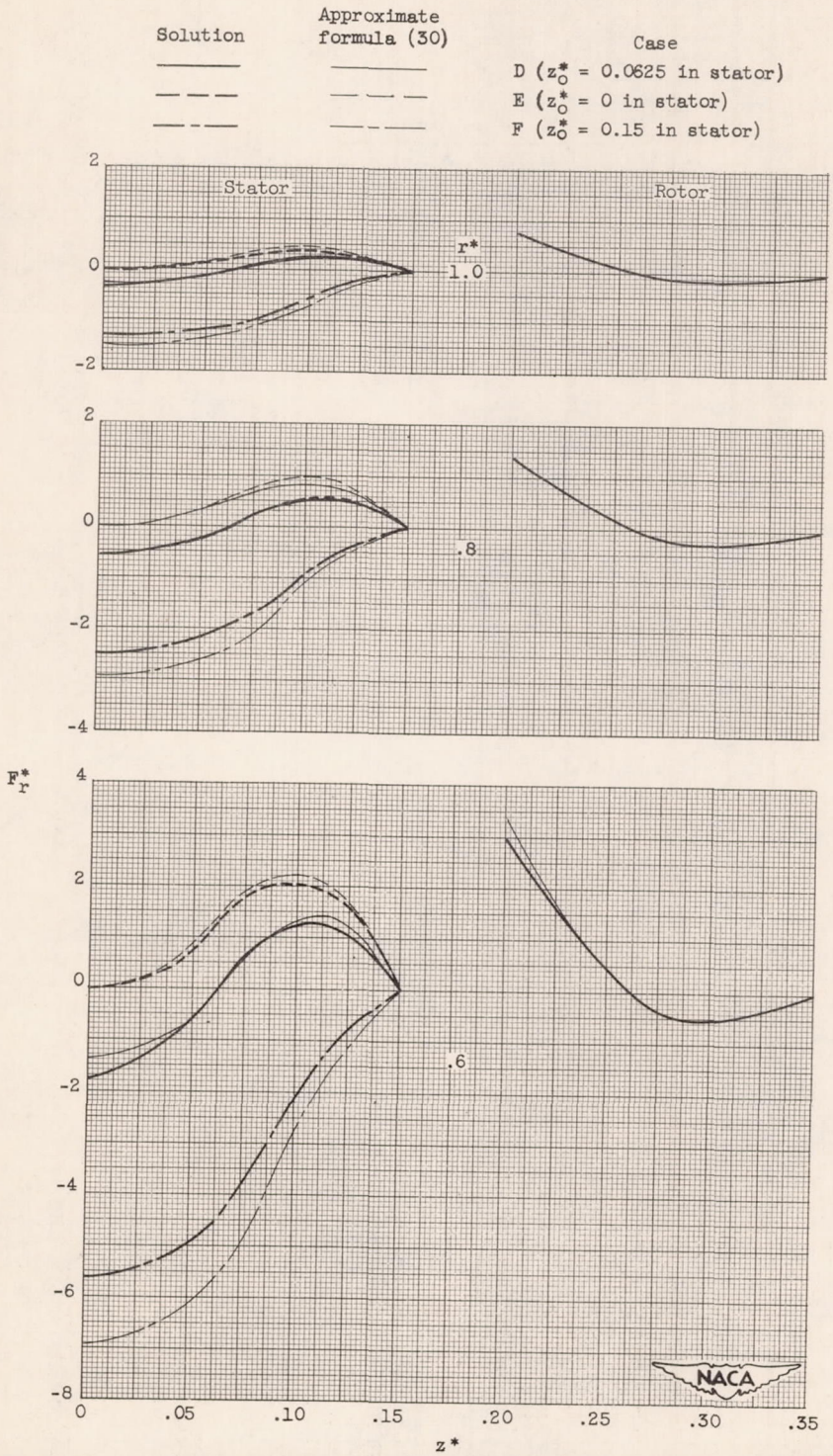

(c) Complete and approximate solutions for F_r^* for cases D, E, and F.

Figure 16. - Concluded. Variation of F in compressible solutions.

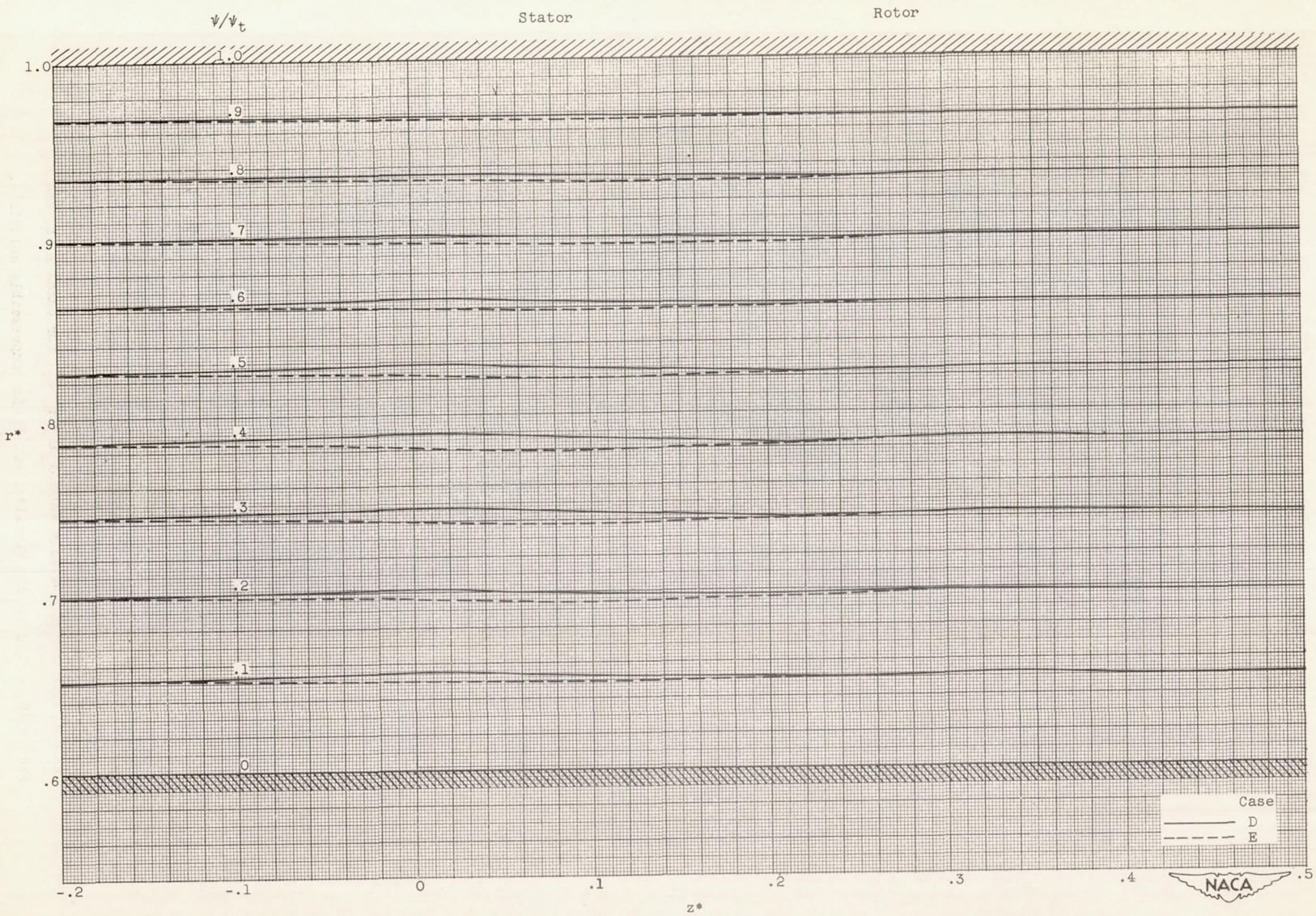

Figure 17. - Meridional projection of streamlines of compressible solutions.

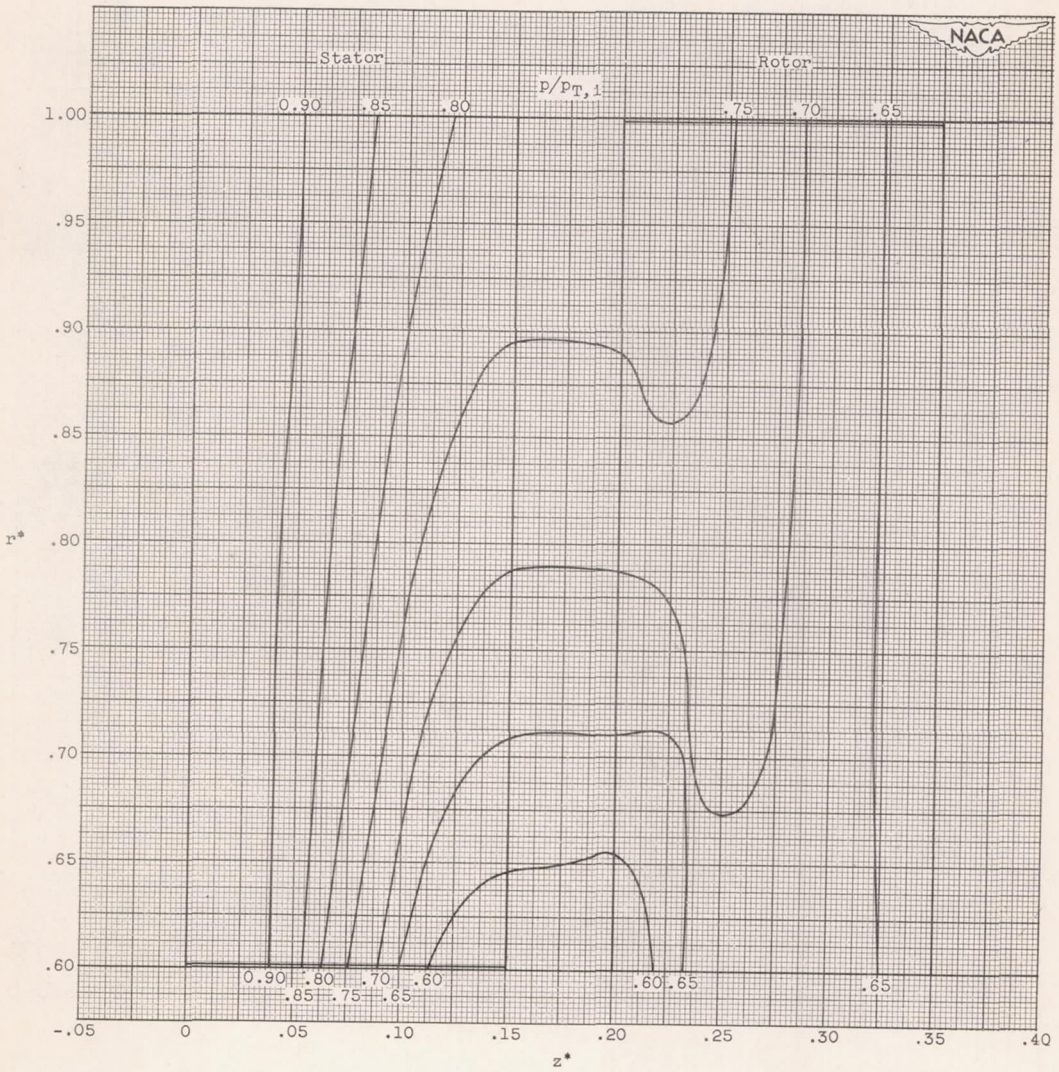

(a) Case D.

Figure 18. - Contours of constant pressure ratio $p/p_{T,1}$.

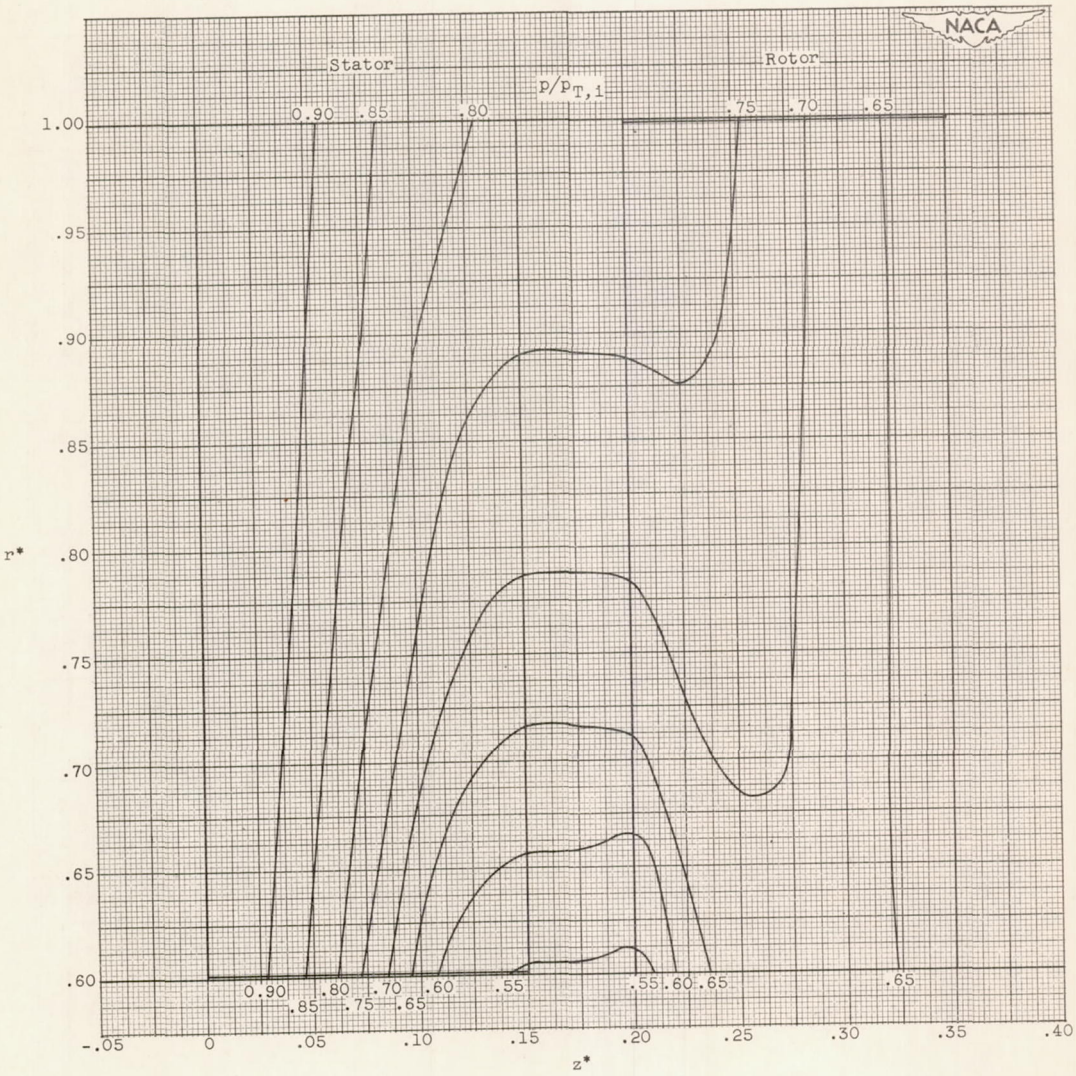

(b) Case E.

Figure 18. - Concluded. Contours of constant pressure ratio $p/p_{T,1}$.

2402

2402

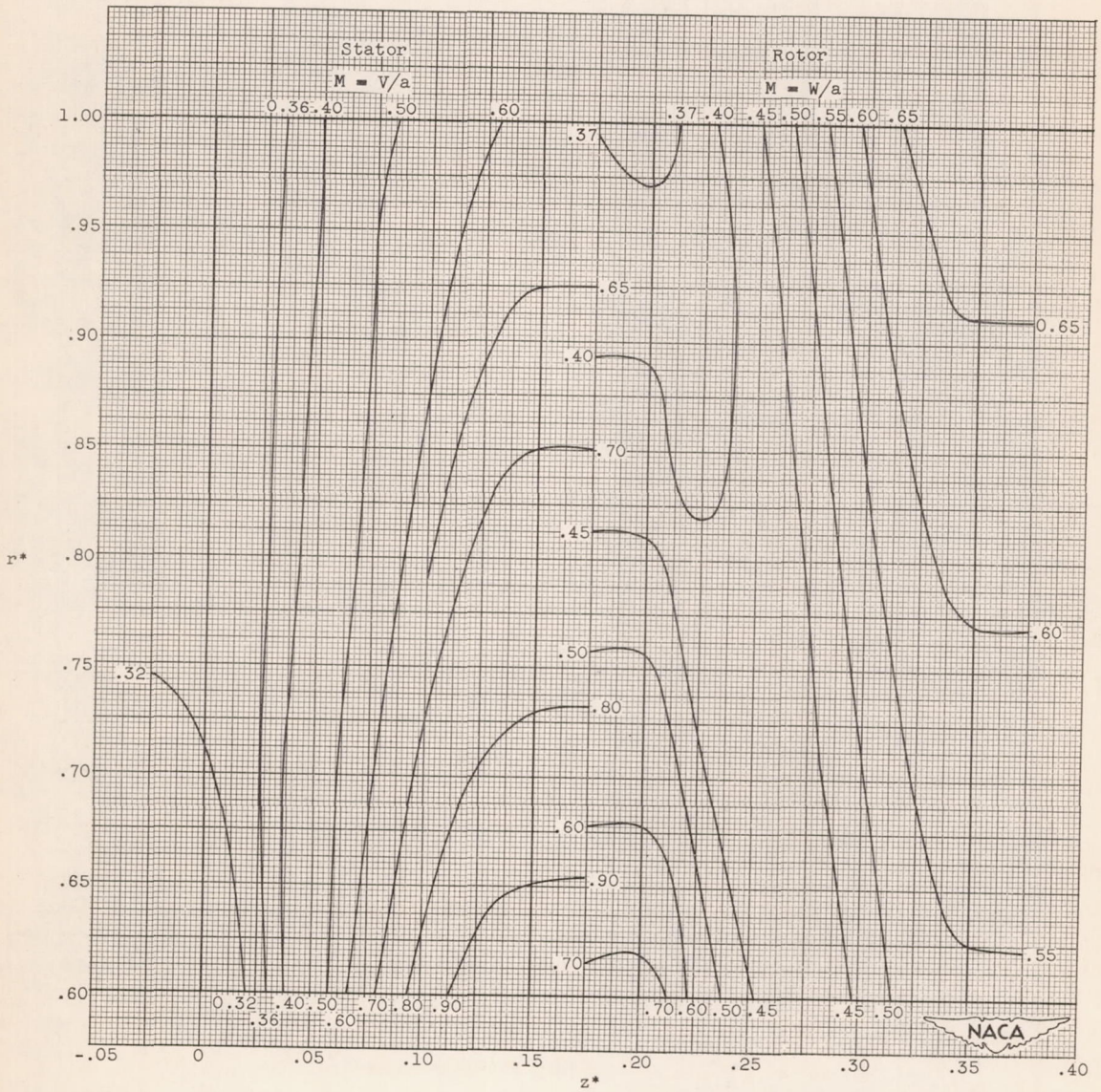

(a) Case D.

Figure 19. - Contours of constant Mach number.

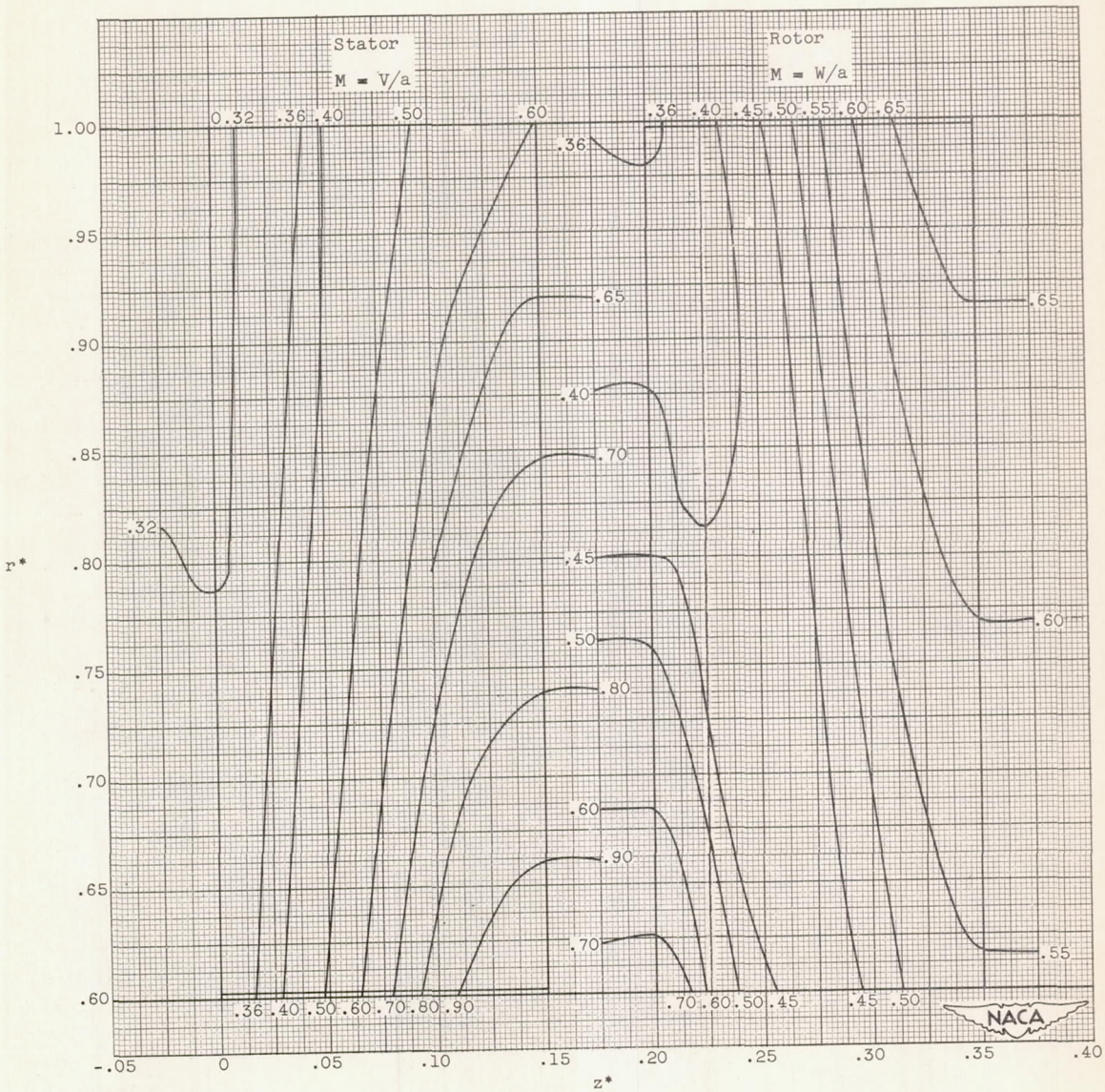

(b) Case E.

Figure 19. - Concluded. Contours of constant Mach number.

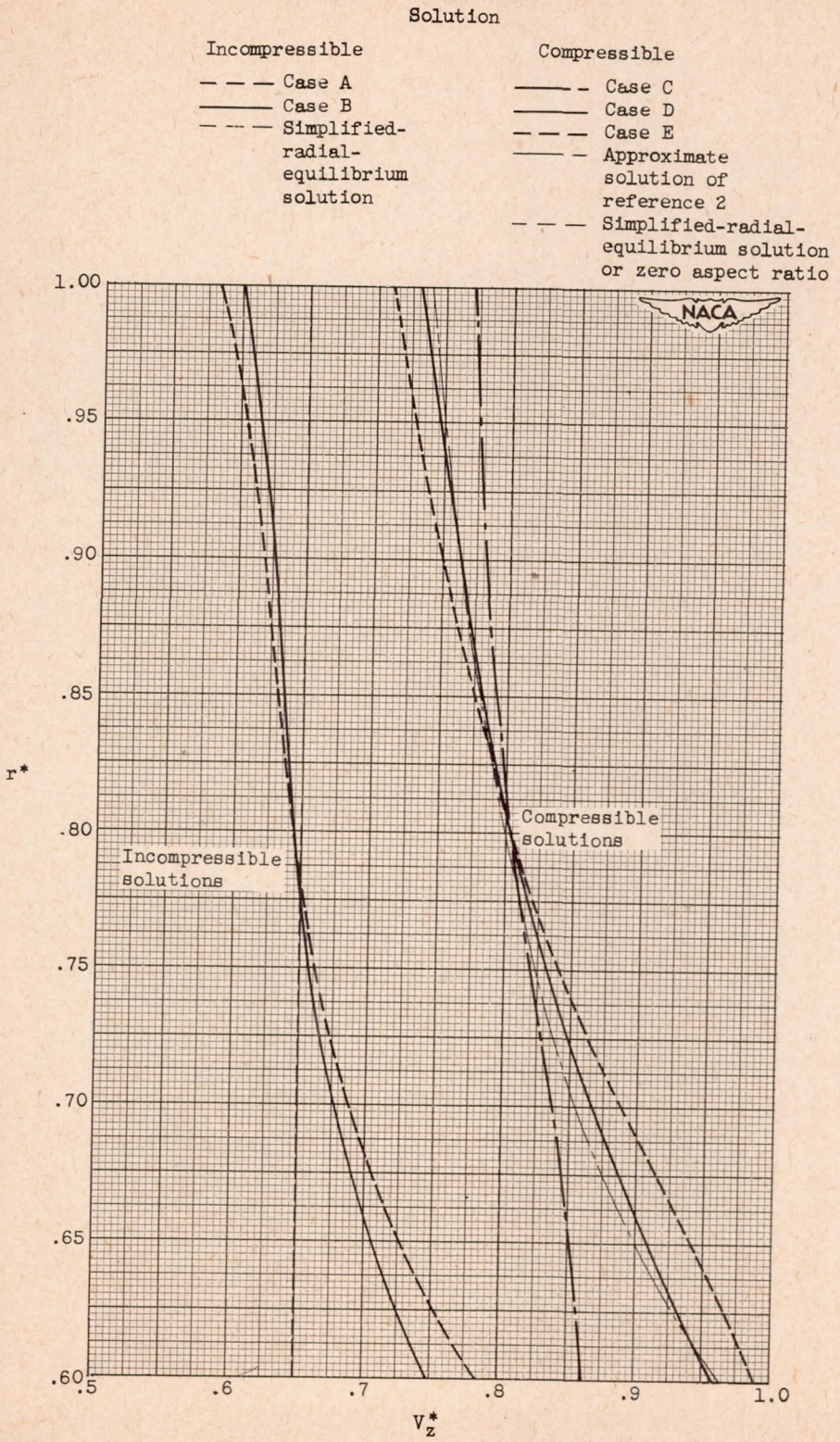

Figure 20. - Radial variation of axial velocity at z* equal to 0.175.